Article

Spatial Variability of Coastal Foredune Evolution, Part A: Timescales of Months to Years

Katherine Brodie [1],*, Ian Conery [1], Nicholas Cohn [1], Nicholas Spore [1] and
Margaret Palmsten [2]

[1] Coastal and Hydraulics Laboratory, U.S. Army Engineer Research and Development Center, 1261 Duck Rd, Duck, NC 27949, USA; Ian.W.Conery@usace.army.mil (I.C.); Nicholas.T.Cohn@usace.army.mil (N.C.); Nicholas.J.Spore@usace.army.mil (N.S.)

[2] U.S. Naval Research Laboratory, Stennis Space Center, Hancock, MS 39529, USA; Meg.Palmsten@nrlssc.navy.mil

* Correspondence: Katherine.L.Brodie@erdc.dren.mil; Tel.: +1-252-261-6840 (ext. 233)

Abstract: Coastal foredunes are topographically high features that can reduce vulnerability to storm-related flooding hazards. While the dominant aeolian, hydrodynamic, and ecological processes leading to dune growth and erosion are fairly well-understood, predictive capabilities of spatial variations in dune evolution on management and engineering timescales (days to years) remain relatively poor. In this work, monthly high-resolution terrestrial lidar scans were used to quantify topographic and vegetation changes over a 2.5 year period along a micro-tidal intermediate beach and dune. Three-dimensional topographic changes to the coastal landscape were used to investigate the relative importance of environmental, ecological, and morphological factors in controlling spatial and temporal variability in foredune growth patterns at two 50 m alongshore stretches of coast. Despite being separated by only 700 m in the alongshore, the two sites evolved differently over the study period. The northern dune retreated landward and lost volume, whereas the southern dune prograded and vertically accreted. At the start of and throughout the study, the erosive site had steeper foredune faces with less overall vegetation coverage, and dune growth varied spatially and temporally within the site. Deposition occurred mainly at or behind the vegetated dune crest and primarily during periods with strong, oblique winds (>~45° from shore normal). Minimal deposition was observed on the mostly bare-sand dune face, except where patchy vegetation was present. In contrast, the response of the accretive site was more spatially uniform, with growth focused on the heavily vegetated foredune face. The largest differences in dune response between the two sections of dunes occurred during the fall storm season, when each of the systems' geomorphic and ecological properties modulated dune growth patterns. These findings highlight the complex eco-morphodynamic feedback controlling dune dynamics across a range of spatial scales.

Keywords: terrestrial lidar; coastal foredunes; storm impacts; erosion; dune recovery; morphodynamics

1. Introduction

Coastal dunes are frequently lauded for their effectiveness at reducing impacts during storms by protecting communities and infrastructure behind them from flooding hazards (e.g., [1,2]). In addition, the ability for coastal dunes to grow naturally, including following storm-induced erosion, provides a natural mechanism which enhances resiliency along low-lying, sandy coastal regions [3,4]. As a result, dunes are increasingly used as a form of nature-based infrastructure in many managed coastal systems (e.g., [5–8]). Understanding the hydrodynamic, aeolian, and ecological processes which contribute to accretional and erosional dune dynamics on management and engineering timescales (days to years) is therefore critical because of the numerous services that dunes provide (e.g., [9]).

Wave contact with the dune is common on intermediate and reflective beaches during major storms, especially during events coinciding with a large storm surge or sea-level anomalies (e.g., [10–13]). While overwash and inundation can occur when total or mean water levels overtop the dune during the most extreme storms, collisional impacts [14] occur frequently during moderate storm events, and result in sand being removed from the dune face and deposited on the beach or transported into the nearshore (e.g., [15]). The mechanisms driving dune erosion are fairly well-understood (e.g., [16]), and the capabilities of simulating spatio-temporal dune erosion are improving [17,18], though tuning parameters for predictive models can vary significantly along the coast [19].

Similarly, there has been a wide range of research focused on understanding the processes contributing to dune growth (e.g., [20]). Research efforts on accretional coastal dune dynamics have been conducted at many geographic locations over a variety of time scales—from milliseconds to millennia—but have primarily been focused on micro-scale aeolian transport processes on time scales of seconds to hours (e.g., [21–24]) and meso-scale foredune dynamics on the time scales of seasons to decades (e.g., [25–28]). Resulting from extensive literature on dune dynamics, the primary physical and ecological drivers of coastal foredune growth are relatively well-understood. Dunes can naturally rebuild after storms and grow through a combination of wind-driven and ecological processes. When there is sediment availability (e.g., [29]), sand is transported from the sub-aerial beach via the wind and deposited in the dune, leading to vertical (aggradation) and/or lateral (progradation) of the dune. For this transport to occur, a threshold wind velocity must be exceeded to initiate saltation. This threshold is dependent on both local bed grain size characteristics (e.g., grain size distribution and armoring) and moisture content. Driven in part by these supply-limiting processes, saturated sediment transport will typically not occur when the fetch length [30–32] is small (e.g., <20 m). The potential for aeolian sediment transport potential and dune growth is generally higher on dissipative beaches, in part because the dry beach tends to be wide (large fetch) [33]. Recent work on dissipative beaches in the U.S. Pacific Northwest also suggests that infragravity-driven swash may deposit sand into dunes during collision regime events, adding to dune growth [17,28]. Conversely, intermediate and reflective beaches generally have coarser grained material and are narrower in width, typically resulting in smaller overall wind-driven dune growth. While these general morphodynamic trends are highlighted in conceptual models by Short and Hesp [33] and Psuty [25], the details of local dune growth depends on the details of grain size properties, beach morphology, ecological characteristics [34,35]), total water levels, groundwater dynamics [36], biological factors [37], anthropogenic influences, wind characteristics, and the antecedent dune morphology (e.g., [38,39]). These controlling factors vary significantly in the alongshore at local to regional scales. For example, the density and species of dune grass has been shown to be important for influencing the dune shape due to sand-trapping capacity—yet these characteristics vary significantly, both in space and time (e.g., [40]).

Wind itself, which is the primary driver of aeolian sediment transport, can also be highly spatially variable. On a local scale, wind variability is driven in part by topographic effects on the flow field, including steering across the dune face [41,42]. For sediment to ultimately be transported from the beach to the dune, there must be a cross-shore component of the wind vector—otherwise, sediment is transported down the coast or into the ocean. Topographically-induced gradients in the wind field and bed shear stress reduction from dune grasses combine to produce local gradients in the transport field, and result in bed deposition or erosion [35,43,44].

Despite the dominant drivers of dune growth processes being qualitatively understood, there are complex eco-morphodynamic feedbacks, scale-dependent processes, and aggregation effects that have precluded accurate simulation of dune evolution across the range of timescales relevant for coastal management (days to years) (e.g., [20,38,45,46]). This represents a gap in the ability to apply research to coastal management problems where coastal foredunes are used as an asset in developing resilient coastlines [47]. Research gaps at intermediate scales, where the aggregation of short time- (<seasonal) and space- (<1 m) scale hydrodynamic, meteorological, and ecological processes are all important drivers of coastal landscape change, contribute to this relatively poor predictive capability of coastal

dune evolution. However, as managed dunes become recognized as important features for coastal protection [48], there is an increasing need to synthesize the relevant environmental, morphologic, and ecological controls on their evolution across the continuum of temporal and spatial scales relevant for coastal management. Improved predictive capabilities of dune erosion, growth, and recovery are critical for the effective management of coastlines throughout the world, particularly in the context of changing environmental forcings (e.g., sea-level rise, changes in storminess) and increased anthropogenic pressures on coastal resources (e.g., [47]).

Limits in data collection techniques have contributed to limitations in understanding the spatio-temporal deposition patterns in dunes at these relevant scales. Historically, aeolian transport processes have been characterized by short (<week) in-situ field studies, ecological processes by infrequent measurement campaigns, and meso-scale dune dynamics through sparse transect-based topography surveys [49] or from intermittent airborne lidar surveys [50,51]. Data frequency and sparseness both pose issues for bridging scales. Recently, high-resolution terrestrial lidar scanners have been utilized to explore beach and dune dynamics at high spatial resolution (centimeters) and, in some cases, with high frequency (e.g., [52–56]). These high-density data provide an opportunity to expand the scientific understanding of complex dune eco-morphodynamics that was not previously attainable.

In this paper, we investigate dune evolution at the U.S. Army Engineer Research and Development Center's Field Research Facility (FRF) in Duck, NC, located on the barrier islands of North Carolina's Outer Banks. High-resolution terrestrial lidar data are used to explore morphodynamic controls on alongshore variable dune growth patterns. Specifically, we use ~monthly lidar scans to quantify topographic evolution and vegetation coverage at two 50 m alongshore stretches of dune within the FRF property. Observed topographic and volumetric responses are compared to forcing conditions (waves, water levels, and wind speeds) in each inter-survey period to gain insights into the drivers of alongshore variability in dune growth patterns. In this manuscript, Section 2 provides an overview of the FRF field site, and Section 3 provides details on the instruments, datasets, and methods used to characterize controls on dune evolution at the study site. Section 4 presents the results of the data analysis. The discussion and conclusions are given in Sections 5 and 6, respectively. This work was conducted as a complementary study to that of Palmsten and Brodie [57], which focuses on the longer term (multi-decadal) beach and dune dynamics at the FRF.

2. Field Site

The FRF is an oceanographic research facility located on the Northern Outer Banks barrier islands of North Carolina, USA, focusing on the collection of oceanographic and morphologic data. The narrow (1 km wide) barrier island is situated between the Atlantic Ocean to the east, and the Currituck Sound to the west (Figure 1a). The facility includes 1 km of a sandy, dune-backed, micro-tidal, intermediate beach with fine to coarse sand [58], and an average foreshore slope of 1:12 [59]. The surfzone is often characterized by one or two sandbars that are frequently longshore-periodic [60], and nearshore morphology is reflective of the recent storm history [61]. The tide range is roughly 1 m, and 0 m NAVD88 is approximately equal to mean sea level (MSL). A local coordinate system for the facility is used in this analysis in which the positive x-axis is aligned with the FRF research pier and directed offshore, and the positive y-axis points 18 degrees west of true north along the beach (Figure 1), with NAVD88 defined as the vertical datum. During the late summer and fall, the region is frequently impacted by tropical low-pressure systems that move north along the U.S. Atlantic East coast. During the winter, cold Arctic air meets the warmer coastal waters of the Gulf Stream off of the North Carolina coast, causing the formation of strong low-pressure systems, called Nor'Easters that track north towards New England. Both types of storm systems can produce storm surge, large waves, and strong winds. The Nor'Easters are characterized by strong winds out of the Northeast, whereas wind direction during the tropical storms (e.g., hurricanes) can be more varied, depending on the storm track. Resulting from the aggregation of wave-driven processes during both calm and energetic conditions, annual net longshore sediment transport along this section of coast is to the

south [62]. A large, prominent dune was constructed (fenced and planted) along the entirety of the Outer Banks barrier islands in the 1930s and 40s [63]. The dunes along the FRF property have been unmanaged since then, and their morphology has been measured regularly since 1981 (See Palmsten and Brodie [57]). During storms, waves frequently impact the dune along the property, but have rarely overtopped the dune since 1980.
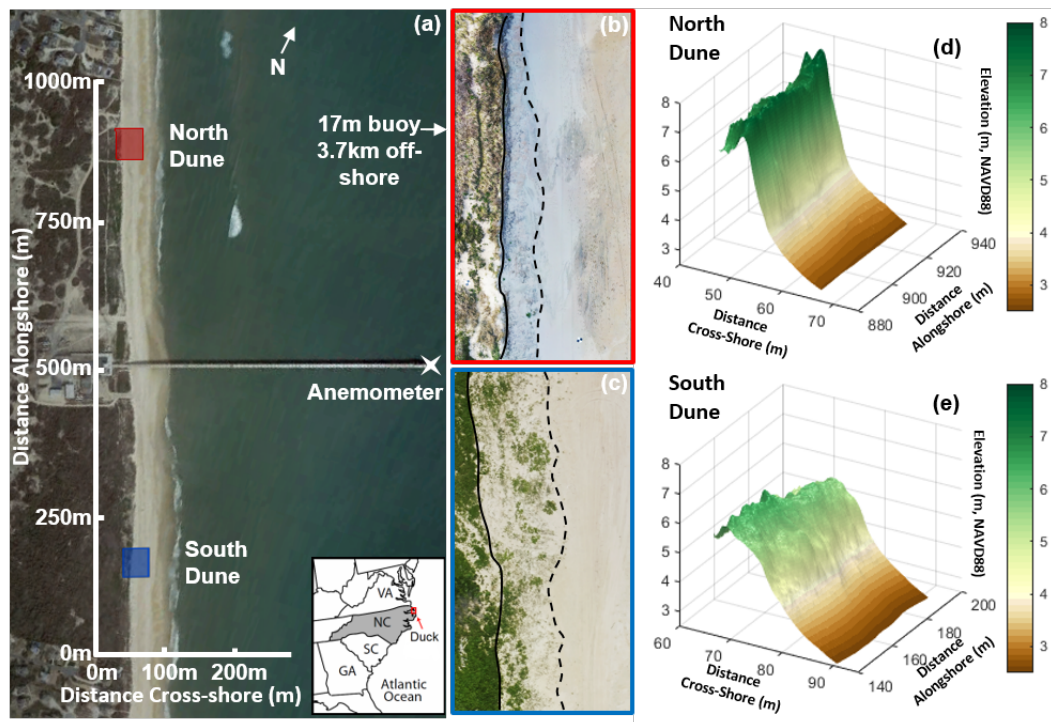

Figure 1. Overview of field sites. (**a**) Aerial imagery of the Field Research Facility and regional inset map. The north dune field site is highlighted in red, and the south dune field site in blue. The location of the anemometer used in this study is shown by the white star. (**b**,**c**) Example high-resolution ortho-imagery with the approximate dune crest (solid) and dune toe (dashed) position indicated, and (**d**,**e**) digital elevation models (colors show elevation in m, NAVD88) of the North and South sites, respectively.

Palmsten and Brodie [57] quantified dune morphology evolution over 25 years along the property, identifying significant differences in the evolution of the dunes on the northern and southern property in the last decade. A similar spatial history of shoreline evolution at the FRF is described in Pianca et al. [64]. These works indicate that while the beach-dune system throughout the FRF property grew for the early part of the observational morphologic dataset, which started in the 1980s, the northern end of the property began experiencing significant erosion in the early 2000s. The dunes on the north side of the property retreated 25 m from 2003 to 2014 (Figure 2a). During this same time period, the southern dunes continued to grow, with a prominent foredune developing from 1990 to 2014 that resulted in the abandonment of the former active foredune (Figure 2b). Dune volume changes were statistically correlated with sub-aerial beach and surf-zone volumes, suggesting that spatial variability in local beach characteristics in the alongshore played a role in the alongshore variable evolution of the dune complex at multi-year time-scales. However, these observations did not have a high enough temporal resolution to identify conclusive relationships to forcing conditions [57].

In this work, we examine two 50 m sections of the dune system at the northern and southern ends of the FRF property (Figure 1), and utilize detailed terrestrial lidar observations to quantify monthly evolution of the two dune systems over a two-year period. The northern study site was located between y = 885 and y = 935 m in the alongshore, and the southern study site was located between y

= 142 and y = 192 m in the alongshore, where distances are expressed in the local coordinate system. Henceforth, the study sites will be referred to as the "north dune" and "south dune", respectively.
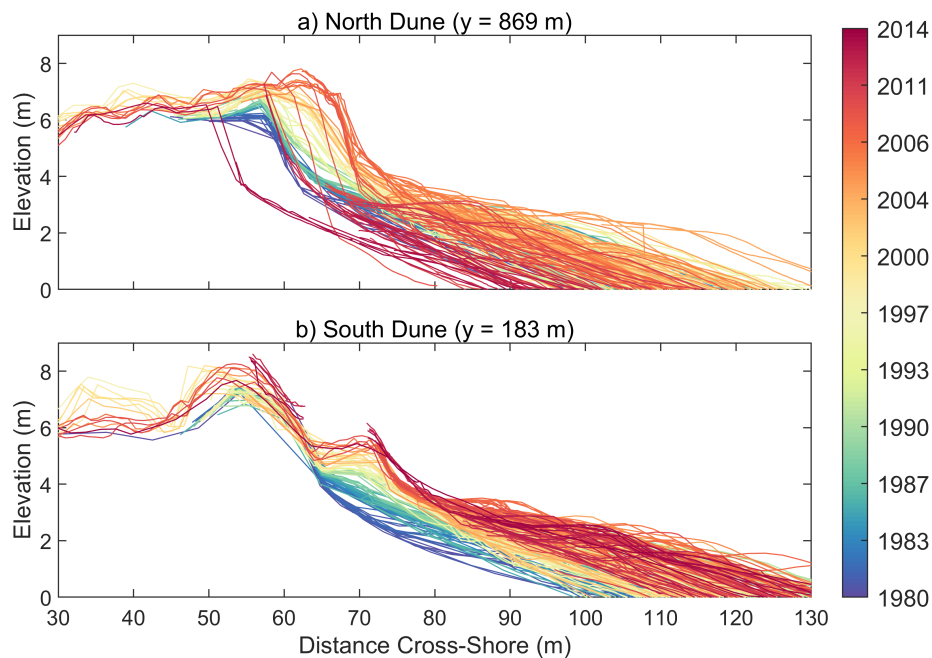

Figure 2. Field Research Facility (FRF) long-term dune evolution. Elevation (m, NAVD88) versus cross-shore position through time (colors increase in time from 1980 (blue) to 2014 (red)) for a cross-shore transect through: (**a**) the northern study site at *y* = 869 m, and (**b**) the southern study site at *y* = 183 m. Profile locations are dictated by standard FRF Profile sample locations.

3. Methodology

3.1. Lidar Data Collection and Processing

Dune morphology was measured at the northern and southern dune sites at approximately monthly intervals (gray dashed lines, Figure 3) from December 2014 through December 2017 using a VZ-2000 terrestrial lidar scanner, manufactured by Riegl Laser Measurement Systems, Riedenburgstrasse, Austria. These data were collected and processed following the same methodology described by Conery et al. [65]. The scanner was mounted on a tripod at five locations within each study site—three on the beach, and two behind the dune (as an example, colors in Step 1, Figure 4 show data from individual scans). Scans were collected with a ϕ resolution of 0.03° (horizontal) and θ resolution of 0.03° (vertical angle). All scans were performed at low tide to maximize beach coverage, and the data collection occurred on non-rainy days with wind speeds of less than 15 m/s to minimize intra-scan movement of the scanner.

Five permanent poles with 10 cm reflective cylinders were installed into the ground near the dune crest and back dune within each site at the start of the study (2015). These poles served as control points for all subsequent scans to tie the lidar-derived xyz point data back to a common reference system. Reflector centroids were surveyed with a real-time-kinematic GPS for 3 min. Each reflector was scanned from each scan location at high resolution ($\phi = 0.005°$; $\theta = 0.005°$), and reflector centroids were identified in Riegl's RiScanPro Software (RIEGL, Vienna, Austria). A least squares minimization between the reflector centroids in the scanner's coordinate system and the local coordinate system was used to determine the rigid transformation matrix needed to rectify data from each scan position. To ensure all the data from each scan position within each survey was aligned to a common reference frame, the easternmost scan position for each site was held static, and each other scan was coregistered to this scan using RiScanPro's plane-matching algorithm. This process accounts for small errors in

the transformation matrices and follows the methodology outlined by LeWinter [66]. An example merged point cloud is shown in Step 2, Figure 4, where the co-registered and merged data are colored by elevation.
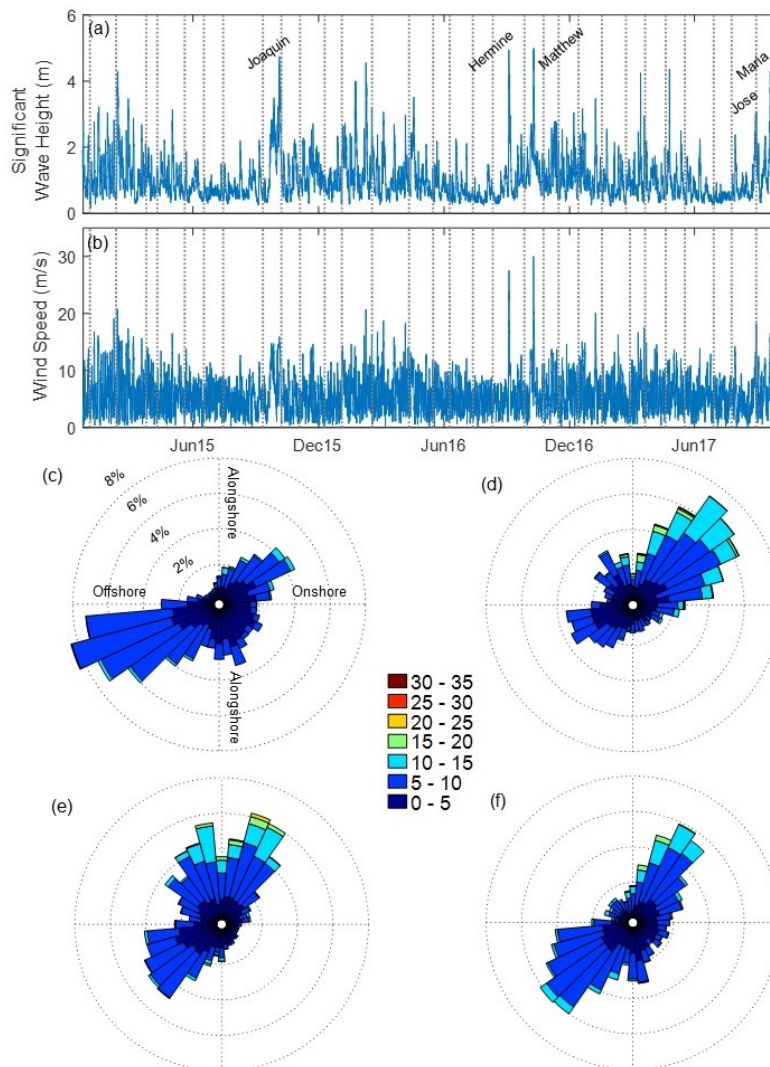

Figure 3. Significant wave height with vertical dashed lines indicating (**a**) survey dates and (**b**) wind speed during the study period. Shore-normal rotated wind roses for the (**c**) summer, (**d**) fall, (**e**) winter, and (**f**) spring during the study period, with colors indicating wind velocity (m/s) and dotted circles indicating percent occurrence.

After all the scans were coregistered to each other for a given survey, inter-survey coregistration was performed to further reduce surveying error. To do so, static features in the field of view, such as nearby houses, buildings, and other structures, were identified in the scans. The rectification of each month's merged scan was updated by minimizing the separation and alignment of planes on the static features in each survey and the first (baseline) survey using a least squares adjustment, similar to O'Dea et al. [55]. Table 1 provides summary statistics from the coregistration process, including the standard deviation (σ) in the final separation of the planes used in the coregistration between each survey and the baseline, indicating that uncertainty in the bare-earth measurements is only on the order of 1 to 2 cm following this robust rectification procedure. This uncertainty is low, relative to conventional real-time kinematic GPS approaches for measuring beach and dune topography (e.g., [67,68]).
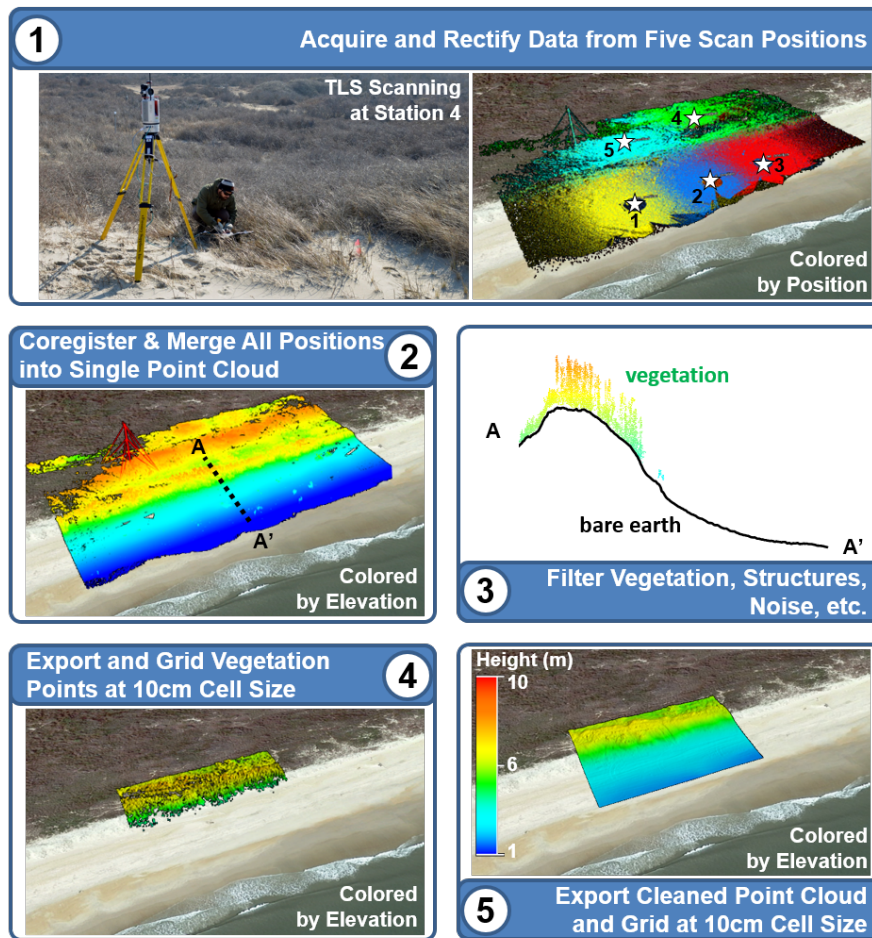
Figure 4. Data acquisition and processing routine for generating Digital Elevation Models (DEMs) used for analysis.

Table 1. Point cloud coregistration statistics.

	North Dune	South Dune
Mean σ (m)	0.018	0.015
Min σ (m)	0.013	0.001
Max σ (m)	0.025	0.020
Mean Number Planes	272	391
Min Number Planes	122	67
Max Number Planes	424	523

Next, a bare-earth surface dataset was generated by removing structures and vegetation. Points that measured vegetation were identified (e.g., green points, Step 3, Figure 4) within RiScanPro using the default vegetation filter settings. The multiple scan positions used within each survey facilitated penetration through the vegetation to the bed in most cases on the dune face. At locations with particularly dense vegetation (e.g., in certain locations behind the dune crest), the true bare-earth was likely obscured, and uncertainty in the bare-earth surface was potentially higher. For this reason, volume changes (defined below) were only calculated on the dune face which had little or sparse vegetation for the north and south dunes, respectively (e.g., Figure 1b,c). In addition, because of contamination by vegetation, deposition analyses behind the dune crest were not conducted in survey intervals which occurred in May, June, and July when vegetation was densest. Note that this spring and summer period also corresponded to the lowest seasonal wind conditions, and thus aeolian sediment transport was likely minimal.

Two data sets were produced for each survey: a bare-earth point cloud and a vegetation point cloud. As final quality control, each bare-earth point cloud was manually checked for erroneous data. Digital elevation models (DEMs) were generated in the local FRF coordinate system with a grid resolution of 10 cm (e.g., Step 5, Figure 4). The vegetation point clouds were also gridded to a 10 cm grid, so that the value at each grid cell represented the average height of all vegetation points at that location (e.g., Step 4, Figure 4). To calculate vegetation height, the DEM was subtracted from the gridded vegetation elevation data. We also quantified the extent of spatial vegetation coverage for each survey for the back dune, foredune face, and upper beach by calculating the percent of grid nodes in each region with vegetation present.

3.2. Morphology Metrics

A variety of metrics were calculated from each survey's DEM to characterize dune morphology at each of the two sites. Dune crest elevation z_c was defined as the highest elevation on the foredune, as calculated from each cross-shore transect at each 0.1 m grid cell in the alongshore (y) direction. The cross-shore position of the z_c location is denoted as x_c. For each cross-shore profile, the dune toe elevation z_t was defined by the location with the maximum curvature between z_c and the mean high water (MHW) contour elevation, similarly to Stockdon et al. [69]. The toe position was made complicated by the occasional presence of upper beach scarps, which formed the above MHW during spring tides or other oceanographic events. The presence of these features caused z_t to artificially shift seaward, and did not appropriately define the lower limit of the dune. Therefore, the cross-shore location of the 4 m contour x_{4m} was also used as an additional proxy for the dune toe location (per Palmsten and Brodie [57]) for the purposes of calculating volume changes. As will be shown, absent of the presence of beach scarps, the 4 m contour is locally representative of the dune toe.

Foredune width w_d was defined as the distance between x_c, and x_{4m}, with the foredune slope β_d defined as the slope of the best-fit linear regression through the cross-shore profile data between x_c and x_{4m}. Foredune profile volume V_d was also calculated as the integrated area over the fixed cross-shore region between x_c and x_{4m} of the initial survey. For all metrics, the alongshore-averaged quantity is henceforth denoted with an overline (e.g., $\overline{V_d}$), and changes in metrics between intervals will be identified with a δ (e.g., δV_d). To account for variability in the temporal frequency of surveys, monthly change rates were normalized by the ratio of the number of days between each survey to 30. Vertical aggradation rates ($\delta z / \delta t$) for each grid cell were calculated by fitting a linear trend through elevations from the combined survey data. Similarly, horizontal contour change rates ($\delta x / \delta t$) were calculated by fitting linear trends through all of the cross-shore topographic data for each DEM grid node in the alongshore. These change rates, which reflect progradation or recession, were calculated for every 0.1 m in the vertical.

3.3. Wind and Wave Data

Standard meteorological variables and a wide range of oceanographic parameters (e.g., waves, currents, tides) were continuously collected at the FRF (Figure 3). Here, a single wind gauge located at the end of the FRF pier (elevation of 18.9 m) and a wave buoy located in a water depth of 17 m were used to quantify the environmental forcing factors contributing to dune evolution (Figure 2).

The nearly continuous significant wave height (H_s, Figure 3a) and wave period (T) measurements were used to calculate wave power (P) as:

$$P = \frac{\rho g^2}{64\pi} H_s^2 T \tag{1}$$

where ρ is the water density, and g is gravitational acceleration. Wave power was then integrated across each inter-survey period ($\int P$). This metric provides a proxy for offshore wave energy, where energetic conditions are typically thought to be erosive to the beach and potentially the dune, whereas calm periods are typically associated with accretive beach conditions (e.g., [28,70,71]). During the study

period, five named tropical storms (Joaquin, Hermine, Matthew, Jose, and Maria) and five Nor'Easters with H_s exceeding 4 m impacted the area.

The local wind time series (Figure 3b) was used to constrain the potential for accretive dune conditions. Both wind speed (u) and wind direction (θ) were measured at the pier (Figure 3b–f). Since aeolian sediment transport rates are generally related to wind speeds to a power greater than 1 (often 3), here, the cubed wind velocity was also calculated ($\int u^3$) for each inter-survey period to inform the aeolian transport potential. The wind direction relative to the shoreline also plays a large role in controlling sediment supply to the dune, affecting apparent fetch lengths and foredune face slopes, and thus may influence the location and magnitude of deposition [38,72]. To quantify wind direction during each survey interval, i, the weighted average wind direction, θ_i, was calculated using the wind speeds, u_j, as weights:

$$\theta_i = \frac{\sum\limits_{j=1}^{n} u_j \theta_j}{\sum\limits_{j=1}^{n} u_j} \tag{2}$$

where j is each hourly wind observation, and n is the number of hours within each survey interval.

At the FRF, the summer wind climate (Jun-Aug; Figure 3c) is generally characterized by mild conditions and dominated by offshore winds out of the SW. In the fall (Sep-Nov; Figure 3d), the passage of tropical systems and the occasional early season Nor'Easter dominate the wind climate, with storms generally characterized by onshore oblique winds out of the northeast. In the winter (Dec–Feb; Figure 3e), winds are strong and predominantly alongshore, where out of the North and in the spring (Mar–May; Figure 3f), the wind climate is bi-modal with a mix of light, summer-like offshore winds and the occasional strong onshore Nor'Easter. During the study period, wind velocities exceeded 20 m/s during five events (Nor'easter in February 2015; Nor'Easter in February 2016; Hurricanes Hermine and Matthew in September and October 2016; and a Nor'Easter in January 2017).

3.4. Eco-Morphodynamic Analysis

To investigate the relationships between morphology, ecological characteristics, and environmental forcing conditions driving the spatial and temporal variability in dune growth within each site, we characterized the response and forcing conditions during each deposition interval for each 0.1 m spatial grid cell within the north and south dune systems. For each cell, we identified survey intervals where net deposition exceeded 0.05 m in the vertical to select events where measurable accretion occurred. For each cell meeting these criteria, we calculated the time-averaged magnitude of deposition, $\langle \delta Z_i \rangle$, over each survey interval, as well as the number of intervals, N_d, that met the deposition criteria. For each cell, we also quantified the time-averaged wind direction during the measurable deposition intervals, $\langle \theta_d \rangle$. To appropriately average the wind direction during each deposition interval in time, each interval's θ_i was weighted by its δZ_i as follows to quantify the dominant wind direction corresponding to local cell deposition:

$$\langle \theta_d \rangle = \frac{\sum\limits_{i=1}^{N_d} \delta Z_i \theta_i}{\sum\limits_{i=1}^{N_d} \delta Z_i} \tag{3}$$

Since the presence of vegetation is likely one of the main contributing factors for reducing wind speeds leading to the deposition of sediment on the dune [34,35], we also calculated the average vegetation coverage, $\langle VC_d \rangle$, for each bin during the interval of deposition. $\langle VC_d \rangle$ was defined as the percentage of bins with vegetation present in a square meter centered on each bin, during each interval of deposition.

To compare these metrics between sites, we calculated alongshore averages of the time-averaged deposition magnitude, $\overline{\langle \delta Z_i \rangle}$, deposition frequency, $\overline{N_d}$, wind direction, $\overline{\langle \theta_d \rangle}$, and vegetation coverage $\overline{\langle VC_d \rangle}$. For both $\overline{\langle \theta_d \rangle}$ and $\overline{\langle VC_d \rangle}$, averages in the alongshore were weighted by the magnitude of the deposition at each grid location. To directly compare these quantities for the north and south dunes, we also defined a normalized cross-shore dune position, X_N, relative to the dune crest position as:

$$X_N = \frac{x_c - x}{x_c - x_{4m}} \tag{4}$$

4. Results

4.1. Dune Characteristics

The north dune was tall (7.18 m $< z_c <$ 7.55 m), narrow (4.01 m $< w_d <$ 6.42 m), and steep (0.42 $< \beta_d <$ 0.92) (Figure 5a,c), whereas the south dune was shorter (6.03 m $< z_c <$ 6.26 m) and wider (8.08 m $< w_d <$ 9.75 m) with shallower foredune slopes (0.24 $< \beta_d <$ 0.30) (Figure 5b,d). The cross-shore location of the dune crest was fairly alongshore uniform at each site, suggesting that they were characteristically linear, as opposed to hummocky, foredunes (Figure 5a,b). The crest elevation did, however, change with time. As the south dune prograded horizontally and aggraded, the front face of the foredune overtook the original dune crest in many locations (e.g., Figure 5d). Conversely, at the northern site, the x_c retreated landward in many locations, coincident with the deposition of sediment landward of x_c (e.g., Figure 5c).

Despite the differences in inter-site foredune morphology, z_t was similar between the two sites for the duration of the study period calculated using standard concavity-based approaches (South $\overline{z_t} = 3.94$ m $\pm$ 0.20 m(1σ); North $\overline{z_t} = 4.35$ m $\pm$ 0.32 m(1σ)), supporting the choice of the 4 m contour as a characteristic dune toe proxy. In the north, x_{4m} retreated a few meters along much of the study site over the 2.5 year period, whereas in the south, x_{4m} exhibited less temporal variability ($|\Delta x_{4m}| \sim < 1$ m) over the same time period (Figure 5a,b). The north dune's foredune face eroded $\sim$1 m on average. While the northern dune face was mostly erosive, at the southern end of the site, portions of the foredune face were characterized by net accretion ($y < 900$ m). The majority of sand accumulation in the northern dune complex instead occurred landward of the dune crest. In some places, this growth exceeded 1 m, as noted by the blue colors at the northern and southern extents of the site in Figure 5a, although the accretion was not distributed equally in the alongshore. These concentrated areas of accretion typically accumulated on unvegetated lobes on the north dune (Figure 5e). In contrast, the south dune's foredune face grew vertically ($\sim$1 m) over the study period along the entire alongshore stretch of the 50 m study site (blue colors; Figure 5b). Interestingly, the largest dune erosion at the south site was observed landward of the dune crest and was likely associated with disturbances to the vegetation.

Vertical aggradation rates ($\delta z/\delta t$) varied in the cross-shore and between sites (Figure 6a,b). Behind the dune crest, aggradation rates at the north dune were positive ($0 < \delta z/\delta t < 0.04$ m/month; Figure 6a), whereas at the south dune, aggradation rates behind the crest were near zero ($-0.01 < \delta z/\delta t < 0.01$ m/month; within the noise of the data; Figure 6b). Horizontal progradation or recession rates ($\delta x/\delta t$) distinctly varied with elevation for each site (Figure 6c,d). On the foredune face, $\delta z/\delta t$ at the north site was on average erosive, but varied considerably within the site ($-0.05 < \delta z/\delta t < 0.03$ m/month; Figure 6a). In contrast, at the south dune, vertical growth on the foredune face was positive and more homogeneous, peaking mid-way down the dune face near 0.02 m/month.
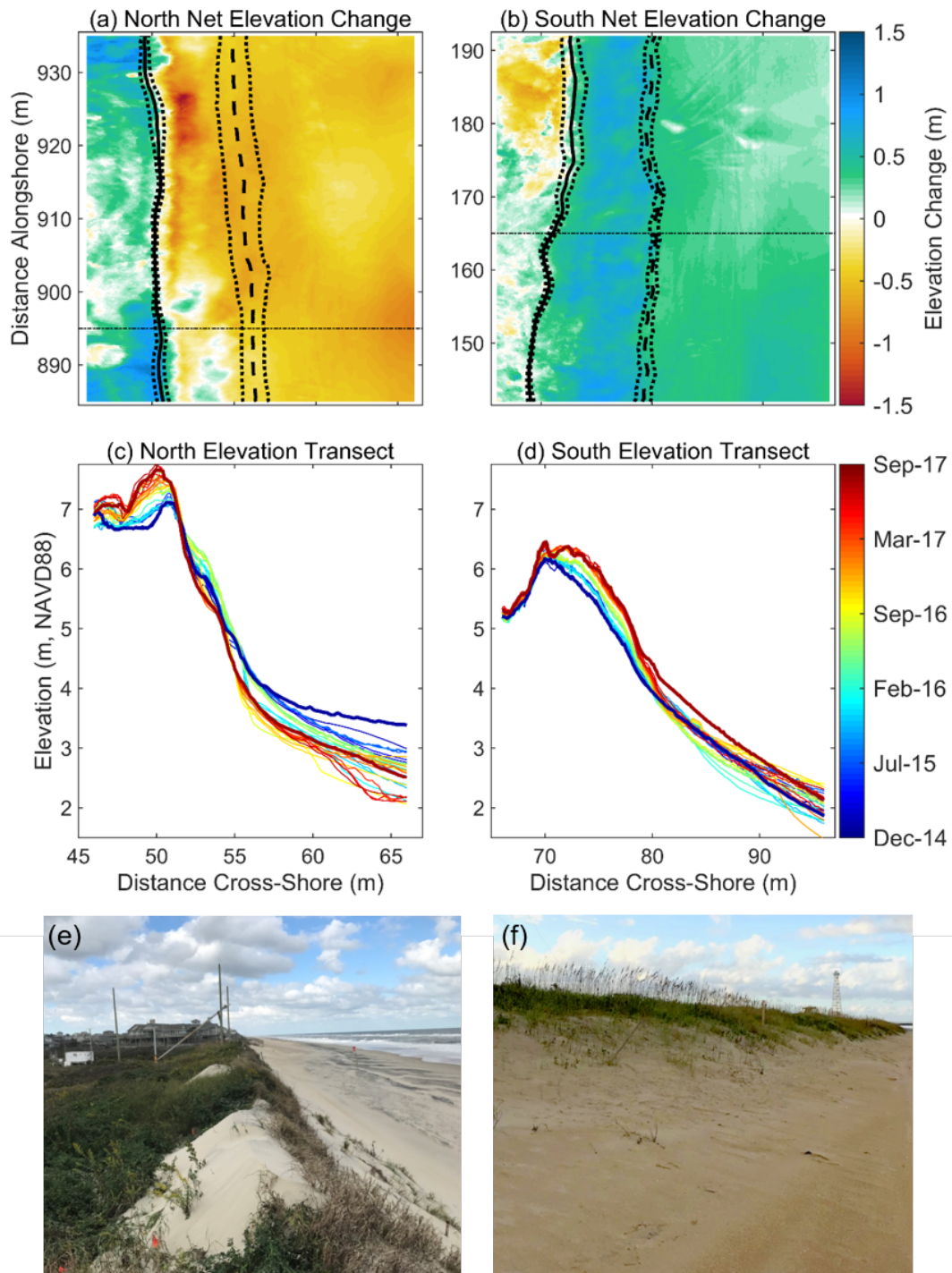
Figure 5. Net morphology change for both sites over the course of the study. (**a**,**b**) Vertical bare-earth elevation changes (colors at right) at each cross-shore (x) and alongshore (y) grid cell between the first and last surveys for the north and south sites, respectively. The average cross-shore location of the dune crest, x_c, and dune toe, x_{4m}, are overlain in solid and dashed black lines, respectively, with $\pm 1\sigma$ for each shown in dotted black lines. (**c**,**d**) Elevation versus cross-shore distance for each survey (blue to red colors show time) at $y = 895$ m and $y = 165$ m (thin horizontal black lines in (**a**,**b**) above). (**e**,**f**) Imagery of the north and south dune field sites from Sep 2017. The two unvegetated sand deposits in (**e**) show the areas of deposition near y = 890 and 930 m.
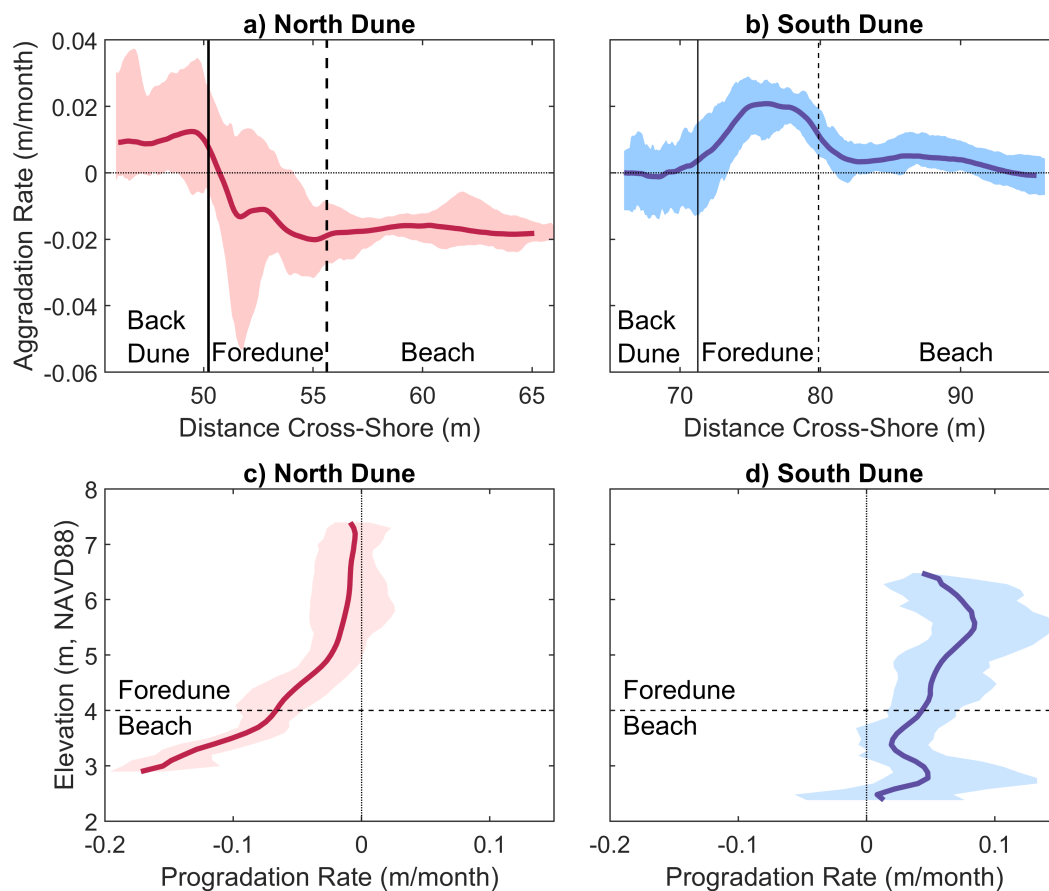
Figure 6. Dune morphology trend analyses. (**a,b**) Alongshore-averaged (solid line) vertical aggradation rates versus cross-shore position for the north and south dunes, respectively. The average cross-shore location of the dune crest, x_c, and dune toe, x_{4m}, are overlain in solid and dashed black lines, respectively, for each site. (**c,d**) Elevation versus alongshore-averaged horizontal progradation rate for the north and south dunes, respectively. For each site, the envelope of variability along the site are shown in the shaded region.

Over the length of the study, $\overline{V_d}$ at the north dune decreased by 2.8 m^3/m, whereas the south dune grew by 4.3 m^3/m (Figure 7a,b). The alongshore-averaged mean volume change rates for the north and south dune were—0.1 and 0.17 m^3/m/month, respectively. These rates varied with time, with both sites experiencing periods of accretion and erosion (Figure 7c,d). At the north site, alongshore averaged foredune volume change rates, $\delta\overline{V_d}$, ranged between -1.36 and 0.44 m^3/m/month (solid red line, Figure 7c). For individual cross-shore transects within the DEM domain, the range of variability was higher, with $-2.31 < \delta V_d < 0.88$ m^3/m/month. There were four main erosive intervals at the North dune, where $\delta\overline{V_d}$ exceeded 0.5 m^3/m/month: February 2015 (large Nor'Easter), October 2015 (Hurricane Joaquin), September 2016 (Tropical Storm Hermine), and October 2016 (Hurricane Matthew). The south dune grew more uniformly over the study period, with fewer erosive intervals. However, growth of the south dune was episodic. There were five intervals where $\delta\overline{V_d}$ exceeded 0.5 m^3/m/month (solid blue line, Figure 7d): February 2015 (large Nor'Easter), March and April 2016 (series of Nor'Easters), October 2016 (Hurricane Matthew), and July 2017. These time periods contributed to 93% of the total observed growth.
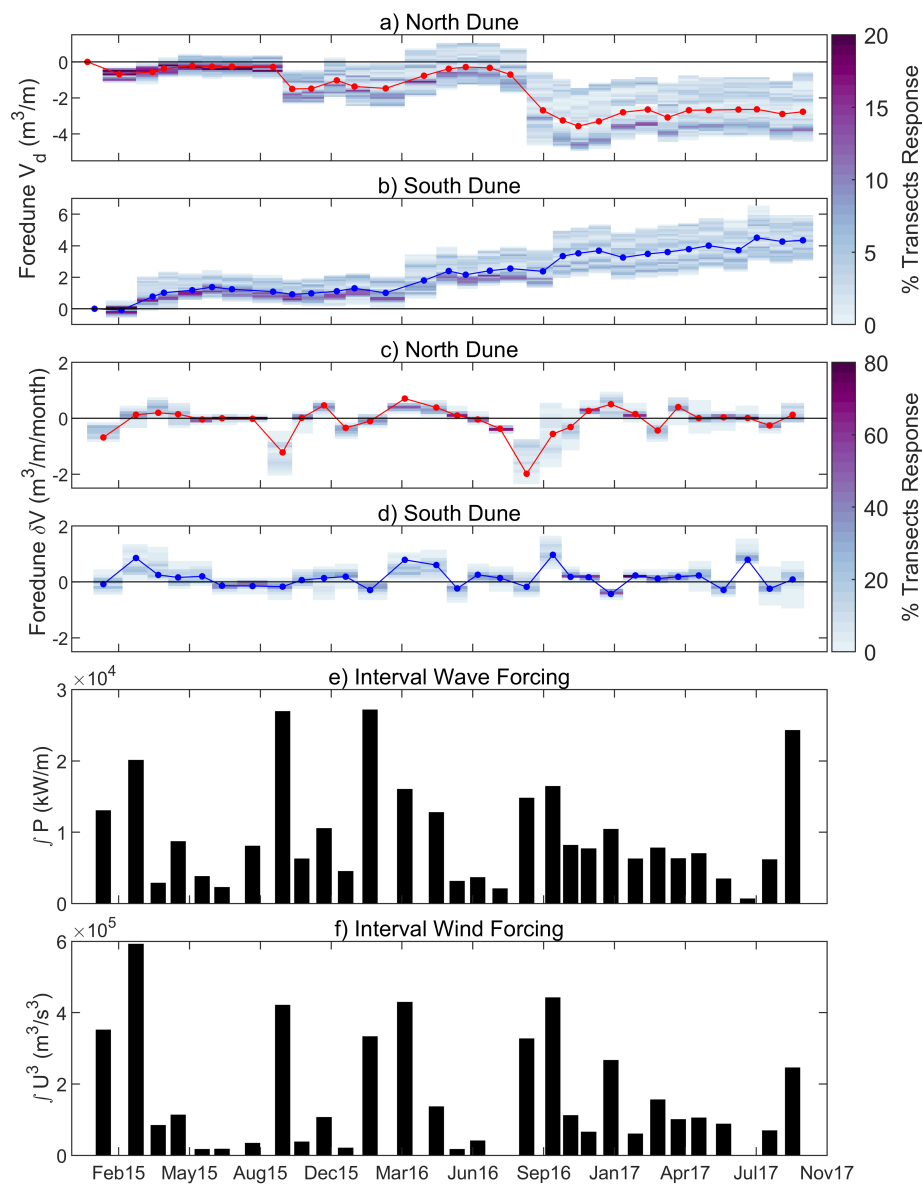
Figure 7. Temporal evolution of both sites over the course of the study. (**a**,**b**) Interval foredune volume, V_d, relative to the first survey and (**c**,**d**) foredune volume change rate, δV_d, through time, for the north and south sites, respectively. Colors show the spatial distribution within the site, and filled circles show the alongshore-averaged quantities, $\overline{V_d}$ and $\overline{\delta V_d}$. (**e**,**f**) Integrated interval wave power ($\int P$) and wind velocity cubed ($\int U^3$) verses time, respectively.

When considering the entire dataset, no direct significant correlations were found between interval foredune volume change ($\delta\overline{V_d}$, Figure 7a,b) and hydrodynamic ($\int P$, Figure 7c) or aeolian ($\int U^3$, Figure 7d) forcing factors. However, at the south site, if considering only intervals when dune growth occurred, alongshore-averaged foredune volume change, $\delta\overline{V_d}$, was significantly correlated to $\int U^3$ (Correlation Coefficient, $R = 0.68$, $p = 0.001$). At the north site, when only considering intervals when erosion occurred, $\delta\overline{V_d}$ was significantly correlated to $\int P$ ($R = 0.84$, $p << 0.001$). The intervals with the strongest winds tended to also coincide with the strongest waves (R between $\int U^3$ and $\int P = 0.83$, $p << 0.001$). In general, storm events tended to erode the north dune (with the exception of winter 2016), whereas storm events tended to grow or have little impact on the south dune.

4.2. Storm Response

As shown above, dune evolution during the study was event-driven, with most of the changes occurring at both sites during the ~6 observation intervals which corresponded to the strongest wind and wave conditions (3 Nor'Easters and 3 tropical systems: Joaquin, Hermine, and Matthew). Elevation changes during each of these intervals varied spatially both within each site and between the north and south dunes (Figure 8). With the exception of Hurricane Joaquin (Figure 8d), all of these events were net accretive to the south foredune, with deposition focused in patchy regions, sometimes resembling ridges, on the foredune face. While the beach changed markedly at times (either growing or eroding) during these events, wave impacts to the south dune were minimal. In contrast, waves impacted the north dune during Joaquin, Hermine, and Matthew (Figure 8c,i,j), causing significant and widespread scarping and erosion along the entire site. However, the response of the north dune to the Nor'easters was more varied (Figure 8a,e,g). Portions of the foredune face during these events either eroded or accreted, sometimes in coherent patterns, suggestive of alongshore bedform migration (e.g., Figure 8a). Deposition also occurred near the dune toe between February and May 2016 at the north dune (Figure 8e,f)–one of the few times during the study when the north dune face gained volume. Video imagery [73] during this time-period confirms that the accretion at the dune toe was derived from aeolian deposition, as opposed to wave-driven deposition, and that the dune toe was not impacted by waves during this interval.

4.3. Vegetation

At the north dune, vegetation was consistently present at and landward of the foredune crest (dark green colors representing nearly 100% vegetation cover behind the gray line, Figure 9a; imagery Figure 5f). The areas with the lowest vegetation cover behind the northern dune crest were located at the northern-most and southern-most bounds of the site, coinciding with the locations of maximum accretion (Figure 5b). The presence of vegetation was more spatially heterogeneous on the dune face. When vegetation was present on the foredune face, it was largely confined to the upper half of the dune, though at times during the spring and summer, annuals also colonized the upper beach face (light brown colors seaward of the black line, Figure 9a and the seasonal patterns in vegetation cover in Figure 9e). An exception to this trend was at the southern end of the north site ($y < 900$), where vegetation near the dune toe persisted for more than 70% of the study (Figure 5e).

At the south site, *Uniola paniculata* (sea oats), which is the dominant grass species at the field site [74,75], and other flora consistently covered the south foredune face for more than 70% of the study (green colors between the black and gray line, Figure 9b; imagery Figure 5a). Similar to the northern site, the area behind the dune crest remained vegetated throughout much of the year, and the beach seaward of the dune toe was rarely vegetated.

Vegetation coverage at both sites varied seasonally (Figure 9e), reaching peaks in coverage in late summer (July/August), and minimums in late winter (February). During the first two summers of this study, the south foredune face had over 70% vegetation coverage. Vegetation was present on at least 50% of the south foredune face during each survey, with the exception of February 2017 when it dropped to 42%. Following this harsh winter, vegetation levels never fully recovered from their February 2017 low period, reaching only 60% spatial coverage during August 2017. In contrast, at the north site spatial coverage on the foredune never exceeded 50% coverage, ranging between 29 and 50% in the winter and summer, respectively. Similarly to the south site, vegetation coverage in summer 2017 was less than during the 2015 or 2016 summers—presumably because of the low winter temperatures.
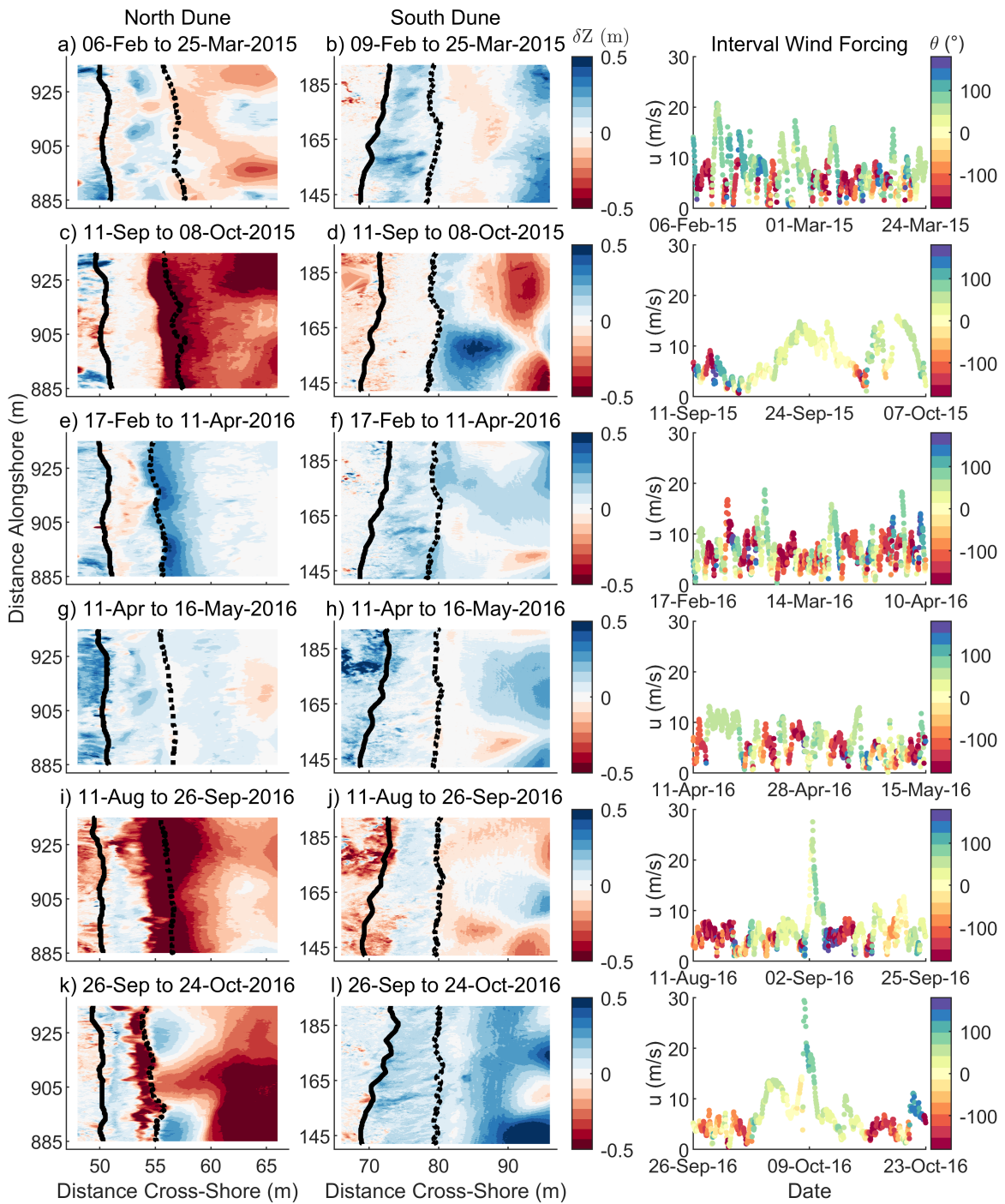
Figure 8. Study site response to storm events. Elevation changes, δZ, for each spatial grid cell for (**a**,**b**) winter 2015 Nor'Easters, (**c**,**d** Hurricane Joaquin, (**e**,**f**) winter 2016 Nor'easters, (**g**,**h**) spring 2016 Nor'easters, (**i**,**j**) Hurricane Hermine, (**k**,**l**) Hurricane Matthew, for the north and south dunes, respectively. The corresponding wind speed, *u* (y-axis) and direction, θ (colors), for each interval versus time is shown in the far right interval.
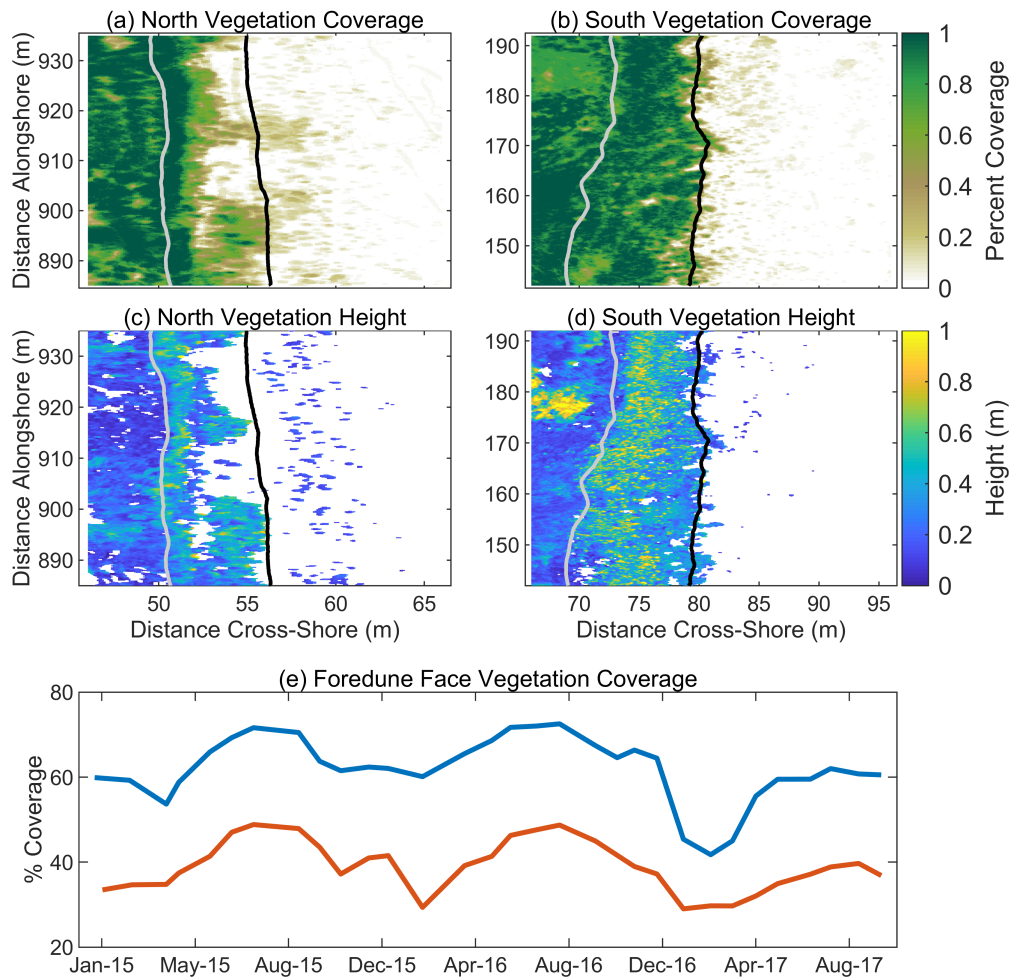
Figure 9. Vegetation characteristics for both sites over the course of the study. (**a**,**b**) Percent vegetation coverage through time (colors top right) and (**c**,**d**) example summer (11 August 2016) vegetation height (m, colors bottom right) at each cross-shore (x) and alongshore (y) grid cell at the north and south sites, respectively. The time-averaged location of z_c and z_t are shown in the gray and black line, respectively. (**e**) Percent coverage of vegetation on the foredune face during each survey for the north (red) and south (blue) sites.

4.4. Temporal Variability in Dune Growth and Vegetation

As discussed in the two sections prior, dune evolution (as quantified by lidar-derived bare-earth elevation changes and lidar-derived vegetation data) at the north site varied in both space and time, whereas the south dune behaved more homogeneously. To highlight relationships between the cross-shore spatial location of dune growth and the extent of vegetation, we examined the temporal evolution of the bare-earth dune and vegetation heights at example profiles for each site (y = 895 m and y = 165 m, Figure 10). The y = 895 m profile within the north dune was selected to examine relationships between morphology and vegetation, as this was one location where vegetation and growth did occur on the foredune face during the study period. However, it is important to note that the response at this example profile is not necessarily representative of the entire north dune site. In contrast, profile y = 165 m within the south site is fairly representative of the entire south dune response, as the dune evolution at the southern site was more spatially consistent.
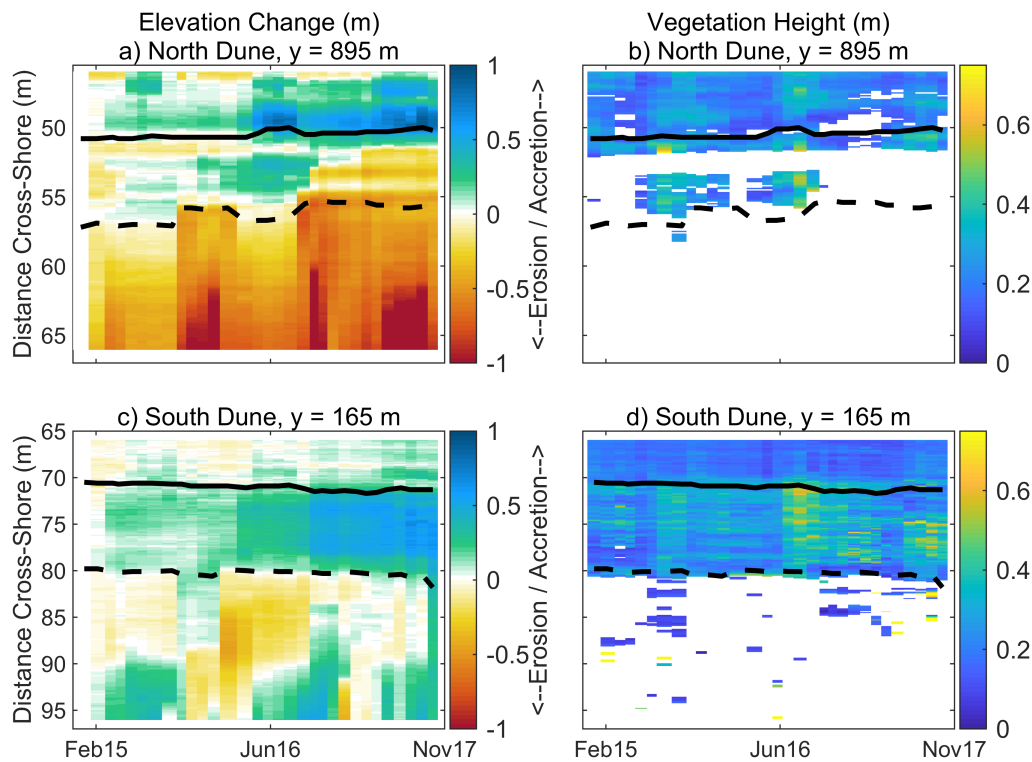
Figure 10. Temporal variability in dune growth and vegetation height at two example transects. (**a,c**) Elevation change since the first survey (colors) at each cross-shore position versus time at $y = 895$ m (**a**, North site) and $y = 165$ m (**c**, South site), respectively. (**b,d**) Vegetation height (colors) through time along the same transects for the north and south sites, respectively. The black solid and dashed lines show the cross-shore position of the dune crest, x_c, and 4 m contour, x_{4m}, respectively.

At both sites, the cross-shore location of dune growth (green colors, Figure 10a,c) corresponds with the cross-shore extent of vegetation on the dune in both space and time (blue to yellow colors, Figure 10c,d). For example, at the north dune site, growth occurred fairly continuously through time landward of the dune crest (solid black line) where vegetation was also consistently present. However, dune growth only occurred on the foredune face when vegetation was present there in summer 2015 and 2016 (compare green colors in Figure 10a between the solid and dashed lines with Figure 10c). In contrast, at the south dune, accretion was focused on the heavily vegetated foredune face continuously throughout the study period (Figure 10b,d). In addition, at the south site, upper beach growth also occurred during the summers when vegetation colonizes seaward of the dune toe (dashed line).

At both sites, some of the seasonal erosion and accretion patterns visible landward of the dune crest on these transects (x < 48 m and x < 70 m for the north and south sites, respectively) may have been due to artefacts in the DEM from dense vegetation that was not fully removed during filtering.

4.5. Intra- and Inter-Site Spatial Variability in Dune Growth

Spatial patterns in deposition in relation to the ecological and morphological properties were directly compared between the two dune systems (Figure 11). At the north dune, the largest ($\langle \delta Z_i \rangle >$ 0.2 m) and most frequent deposition occurred immediately behind the dune crest at the northern and southern ends of the study, near the dune toe and on the lower beach (Figure 11a,c). While deposition near the dune toe was large at times, growth was not persistent here over the course of the study due to frequent wave-driven erosion (Figure 7). Deposition behind the dune crest was largely

confined to ~3 m landward of the dune crest and deposition did not occur frequently on the steep foredune face (Figure 11b), except for y < 900 m, when vegetation was present (Figures 10a,b and 11g). Average wind directions during accretional intervals were highly oblique and in some cases, alongshore, varying spatially between 45 and 100° relative to shore-normal (Figure 11e). Visual observations during high-wind events (not shown) indicated that "jettation" occurred during these strong, oblique winds, with sediment-laden jet-like flows accelerating up the steep, un-vegetated dune face (e.g., [76,77] and transporting sand from the beach to the crest and leeward slope of the dune, consistent with the patterns of deposition behind the dune crest.
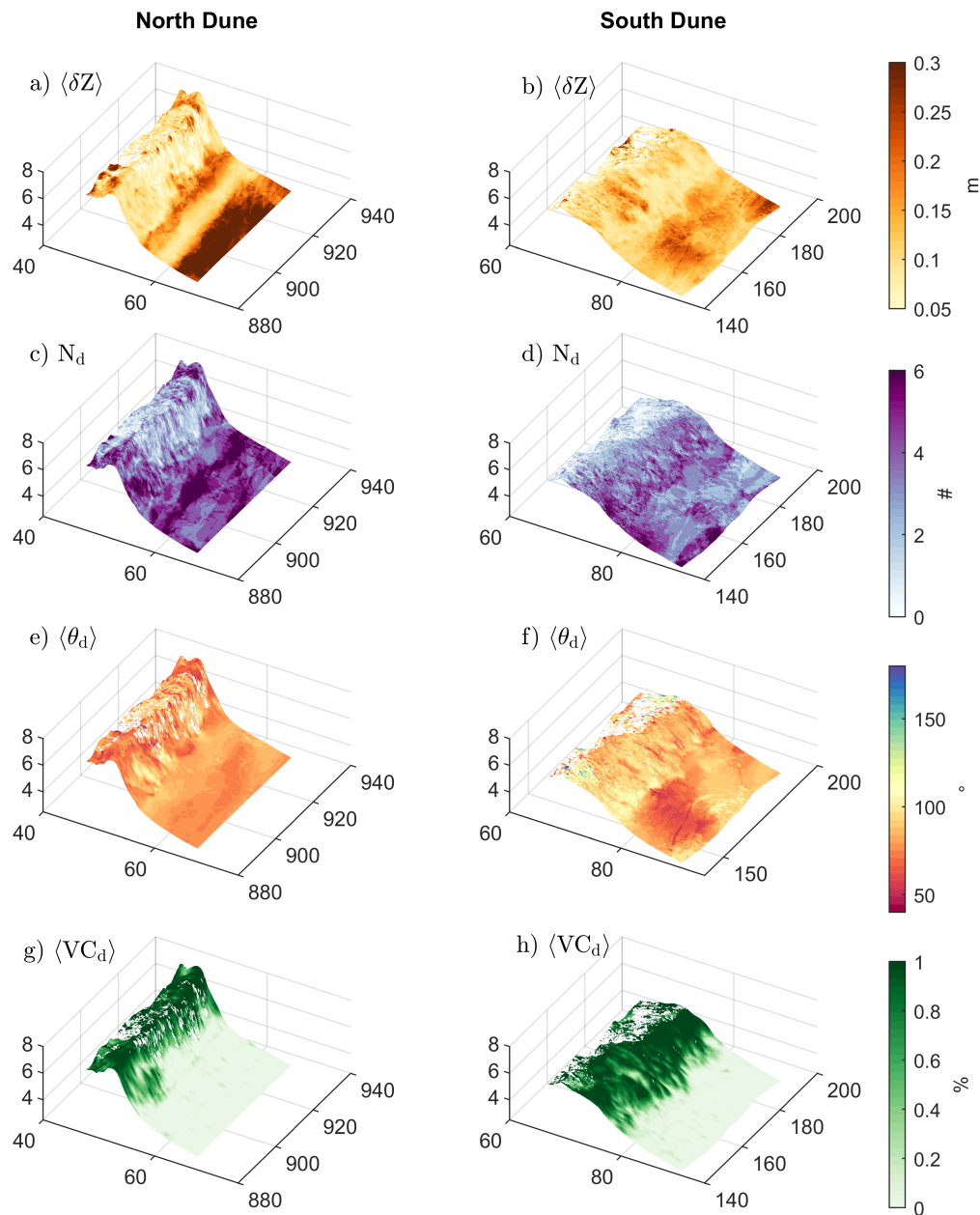

Figure 11. Spatial variability in dune deposition and corresponding forcing factors. (**a,b**) The interval-averaged magnitude, $\langle \delta Z_i \rangle$, and (**c,d**) number of deposition events, N_d, (**e,f**) average wind direction, $\langle \theta_d \rangle$, and (**g,h**) and vegetation coverage, $\langle VC_d \rangle$, as a function of cross-shore position, alongshore position, and elevation, during the deposition intervals for the north and south dunes, respectively. Colors at right show the magnitude of each variable.

At the south dune, the largest ($\langle \delta Z_i \rangle > 0.2$ m) deposition occurred in a few focused locations on the foredune face and on the upper beach (Figure 11b), though most depositional events were of smaller magnitude (0.05 m < $\langle \delta Z_i \rangle$ > 0.2 m) and spread across the dune face. The number of depositional events decreased with increasing elevation on the dune face (Figure 11d), and wind directions during deposition on the dune face were slightly more oblique than for the north dune, ranging from 60 to 120° relative to shore normal (Figure 11e).

Alongshore averaging of the complex spatial patterns also provides additional insights into the drivers of dune evolution within and between the north and south dune study areas. At the north (red lines, Figure 12) and south (blue lines, Figure 12) dunes, average deposition magnitudes were largest at the dune toe near the primary slope break between the upper beach and dune face. At the north dune, deposition in this region most often occurred during periods of highly oblique to alongshore winds, with the winds contributing to deposition at the south dune coming from slightly more onshore than at the north dune (80 vs. 100°). Vegetation coverage near the dune toe during deposition was close to zero for the north dune, and < 30% for the south dune. At the north dune, deposition on the dune face decreased with increasing elevation for the lower 80% of the dune face, until vegetation coverage exceeded roughly 50%, and then increased near the crest, which was nearly 100% vegetated. Deposition near and behind the dune crest occurred with slightly less oblique winds (80°). In contrast, for the south dune, deposition magnitudes on the foredune face were fairly uniform with elevation, with a slight increase once vegetation coverage increased to near 100% roughly 60% up the dune face. Landward of this location, deposition frequency decreased, and deposition behind the dune-crest was infrequent. Deposition near the dune crest on the south dune only occurred during intervals with alongshore winds; winds during deposition became progressively more oblique with increasing elevation on the dune.
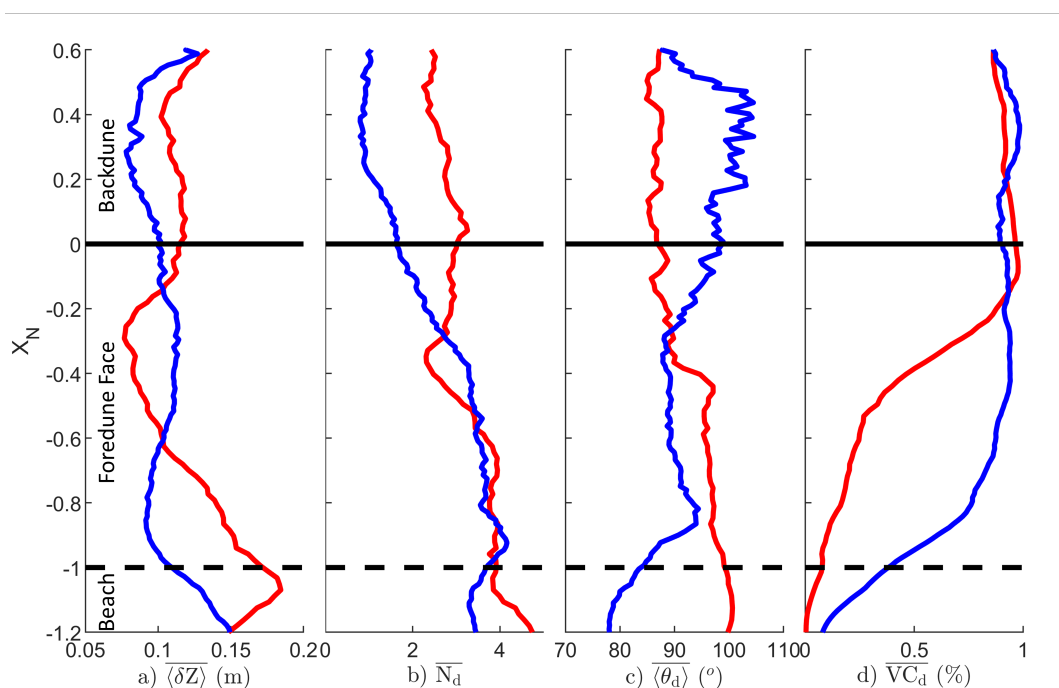

Figure 12. Site-specific trends in deposition characteristics. Normalized cross-shore position, X_N, versus alongshore-averaged (**a**) deposition magnitude, $\overline{\langle \delta Z_i \rangle}$, (**b**) deposition occurrence, $\overline{N_d}$, (**c**) wind direction $\overline{\langle \theta_d \rangle}$, and (**d**) vegetation coverage, $\overline{\langle VC_d \rangle}$ for the north dune (red) and south dune (blue). The dune crest position is shown in a solid black line, and the dune toe position in a dashed black line.

5. Discussion

5.1. Scales of Spatial and Temporal Variability in Dune Evolution

Relatively few studies [53,65**?**] have explored the growth of coastal dunes at spatial scales ranging from sub-meter to tens of meters, and on timescales relevant to coastal management (months to years), despite the recognition that dune growth is critical to maintaining resilient coastlines. Dune evolution is widely described as the cumulative result of complex feedbacks between sediment supply, moisture content, grainsize, vegetation [34,35,40], and topography (e.g., [38,39,41–43])–all of which can vary at these spatio-temporal scales [20].

Deposition was event-driven at both sites, similar to the site in Prince Edward Island, Canada studied by Delgado-Fernandez and Davidson-Arnott [79], with the majority of the net accretion corresponding to only a few survey intervals. The largest dune growth intervals occurred during the stormy season in the winter for the north dune, and fall and winter for the south dune (Figures 7, 8 and 10). At both sites, deposition occurred predominantly during strong, highly oblique, and in some cases alongshore, windy periods, similar to the observations of Davidson-Arnott et al. [72]. Transport from the beach to dune was clearly visible in the field (in both visual observations and in individual images from the continuous coastal imagery tower on-site) during these periods, even when the dry beach width was narrow (<20 m) due to high waves and water levels. The conditions where sediment deposition occurred in the case of offshore directed winds, as measured at the pier location, may reflect the importance of flow reversal processes and complex spatial wind patterns on local depositional processes (e.g., [80]). Deposition patterns also (Figure 8) suggested that alongshore migration of bedforms (e.g., [79]) or localized deflections of the wind field toward the dune by spatially variable beach topography (e.g., [20,81–83]) are necessary to consider when simulating 3D dune evolution at these highly resolved spatial scales. However, topographic measurements at higher temporal frequency simultaneous to wind measurements at higher spatial resolution during large wind events are needed to better elucidate the feedbacks between ecological, morphological, and aeolian processes that drive these complex deposition patterns (e.g., [20]).

Morphologic evolution was spatially complex at both sites, with the north dune showing more variable behavior. Deposition at the north dune predominantly occurred at slope breaks (Figure 11)–either where the flatter upper beach intersected the steep dune face (e.g., the dune toe) or immediately behind where the steep dune face intersected the flatter, vegetated leeward slope of the dune (e.g., behind the dune crest). Despite the deposition at the base of the dune, frequent wave contact with the dune toe over the course of the study resulted in little persistent growth at the beach-dune juncture. In contrast, the deposition behind the dune crest was persistent. While prior work suggests the strongest flow accelerations on the dune face and crest occur during onshore and to slightly oblique winds (e.g., 30°; [84]), our visual observations and measured deposition patterns suggest jettation can still occur during highly oblique wind conditions (e.g., 60 to 90°) on un-vegetated steep dunes. The un-vegetated and lower apparent slope encountered by the oblique winds likely led to flow acceleration, which enabled transport of sand behind the dune crest [76,77,84].

In addition, deposition patterns at our site appeared qualitatively related to vegetation coverage. At the south dune, deposition was concentrated on the highly vegetated foredune face, with deposition frequency decreasing with increasing elevation and increasing vegetation coverage. These patterns suggest much of the sand transported up the dune face is trapped by vegetation lower down on the dune. This serves to reinforce the existing morphology, as sand is mostly trapped on the dune face leading to progradation. Similarly, at the north dune, accretion only occurred on the dune face when vegetation was present on the dune face to trap the sand (Figures 10 and 11). However, during storms, waves collided with the north dune face, rapidly removing vegetation and any recently deposited sand, and preventing persistent colonization and progradation along most of the site (Figure 10). The deposition that did occur behind the dune crest was constrained to within a few meters of the continuously and densely vegetated upper dune face and dune crest. The mostly un-vegetated,

steep dune face allowed sand to be transported to the dune crest, leading to aggradational deposition and reinforcing the taller morphology of the north dune.

5.2. Alongshore Variations in Beach and Nearshore Morphology

While the north and south dune sites were separated by only 700 m in the alongshore, they exhibited markedly different morphological and ecological characteristics as discussed throughout the manuscript (Figures 5, 6 and 9). This included opposing trends in net volume change to the foredune face (Figure 7) and different deposition patterns in the cross-shore (Figure 11) throughout the course of the study, similar to the foredune systems described in Ollerhead et al. [27]. The evolution of the north dune was spatially and temporally variable, but comparable to the evolution of the cliffed stoss slope (CS) dune described and conceptualized by Ollerhead et al. [27]. The behavior of the dune, with persistent deposition generally only focused behind the dune crest, was largely consistent with prior observations characterizing dune retreat and growth during transgression of an erosive coast [20,27,36] when storm impacts are mainly collisional (e.g., no overwash or inundation). In contrast, the south dune behaved similarly to Ollerhead et al. [27]'s stoss slope dune, and instead provides an example of dune progradation, with sand trapped on the foredune face—behavior more characteristic of a prograding coastline with minimal erosional storm impacts.

These spatial trends are consistent with the general foredune behavior over the past two decades, as described by Palmsten and Brodie [57], a companion effort to this work. Focusing on multi-year and decadal scales, Palmsten and Brodie [57] identified that dune volume and sub-aerial and sub-aqueous beach volume were significantly correlated at the FRF, with the behavior of all of these quantities for the north and south dunes changing markedly in the early 2000s. While those data could not identify the specific processes responsible for this spatial variability, Palmsten and Brodie [57]'s results suggest that on intermediate or erosive coastlines where wind and wave events are closely linked and where beach states can vary spatially and temporally, the specific morphology of the beach and surf-zone (slopes, volumes, sandbar positions) prior to a storm can have important effects on total water levels—consistent with the findings at other field sites [17,85,86]. Spatial variability in total water levels relative to antecedent beach and dune morphology can change resultant fetch lengths and frequency of wave collision events, and therefore exert a strong control on dune evolution on spatial scales of tens to thousands of meters.

During the focused measurement period in this study (2015–2017), bathymetric data offshore of the north and south dunes were collected roughly monthly using the FRF's amphibious vessels (Figure 13a). Similar to Palmsten and Brodie [57], the southern region had larger nearshore sediment volumes (as defined in Palmsten and Brodie [57]) when compared with the northern region, with on average 0.6 m shallower water depths across the nearshore. While the average sub-aerial beach slope (defined as the best fit linear trend between the shoreline and 4 m contour) and beach width (defined over the same region) showed no significant differences between the north and south regions, the shoreline in the south experienced significantly less variability than in the north (Figure 13b). These data support the findings of Palmsten and Brodie [57]) that alongshore variations in nearshore processes may play an important role in influencing dune evolution at the FRF through the modulation of wave run-up and/or sediment availability for aeolian transport. As the two sections of dune in this study are in close proximity to one another, and therefore exposed to the same general environmental forcings (offshore waves, tides, surge, and winds) yet experience differing dynamics, it may be that the dune dynamics are closely coupled with nearshore dynamics even on short (<annual) time scales. However, more morphological and process-measurements are needed to understand these nearshore-beach-dune interactions.
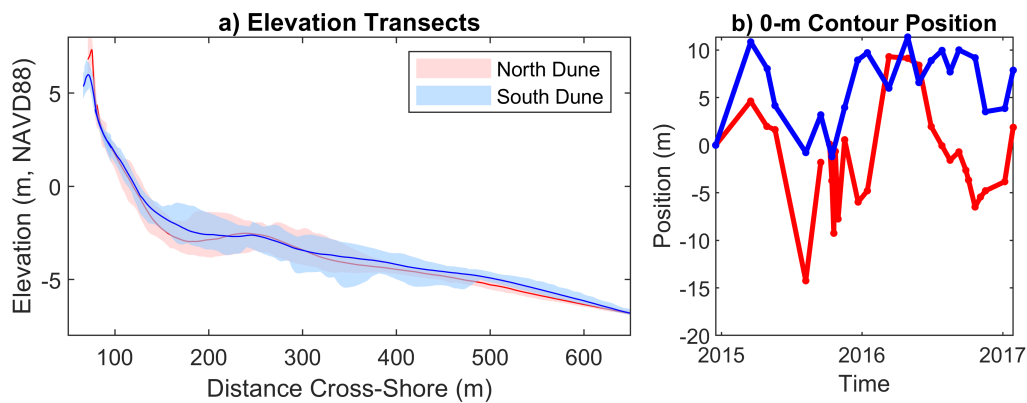
Figure 13. Beach and surf-zone behavior offshore of the north and south dune. (**a**) Average elevation versus cross-shore position for the north (red solid line) and south (blue solid line) profiles during the study. The profile envelop at each cross-shore locations is shown in the shaded regions. The cross-shore location of the north data has been shifted seaward by 25 m so that the mean position of the 0 m contour over the course of the study aligns for comparison purposes. (**b**) The cross-shore position of the 0 m contour for the north (red) and south (blue) regions relative to their respective initial position versus time.

5.3. Implications for Management

While the complex spatial and temporal scales of dune evolution characterized in this work have important scientific implications for understanding dune eco-morphodynamics, the details of dune evolution at these scales can also be important to home-owners and have clear implications for coastal management. For example, at the meeting summarized in Elko et al. [47], home-owners in the town of Nags Head, NC (20 miles south of the FRF) complained of large quantities of sand that were being blown over the dune crest and in-filling pools, covering decks, and impacting homes during energetic wind events—similar to the observed deposition patterns at the north dune during this work. At other sites in the Outer Banks, community members have also voiced complaints of sand rapidly infilling their dune walkovers, having a longer walk to the beach, and no longer being able to see the ocean out of their first story windows due to recent dune growth—descriptions consistent with the aggradation and progradation observed at the south dune site during this work. In contrast, homeowners from the towns of Kitty Hawk, NC (5 miles south of the FRF) and immediately north of the FRF in Duck, NC [87] continue to struggle with severe dune erosion and damage during storms. These various accretional and erosional dune processes have important implications for regional coastal management decisions on the Outer Banks.

The high-resolution terrestrial lidar measurements collected in this study demonstrate the important role of dune grasses on trapping wind-blown sediment and its potential beneficial use in dune management. Consistent with numerous other works (e.g., [65,88–90]), grass planting may be an effective measure in limiting aeolian transport to homes adjacent to the beach and enhancing coastal resilience to flooding by promoting natural dune growth (Figures 9, 10 and 12). However, morphological feedbacks similarly have an important role in influencing dune dynamics (Figures 7, 8 and 13). Synthesizing the competing effects of these complex eco-morphodynamic processes (Figure 8) and aggregating the effects of these processes over time scales relevant to coastal managers (days to years), necessitates quantitative approaches. New coupled numerical modeling tools provide a means to simulate and explore these eco-morphodynamic processes, although these tools still lack many relevant physics and require significant validation and testing across morphodynamic regimes [38,39,44]. High-resolution datasets of morphology and ecology evolution, such as those presented here, which bridge numerous spatio-temporal scales, provide a means to both improve understanding of these complex eco-morphodynamic processes and to test and improve predictive modeling tools. An improved understanding of the processes driving spatial variability in dune

evolution on scales of meters to kilometers is critical for effective management of coastal regions, especially along erosional coastlines such as the Outer Banks.

5.4. Value-Added from High-Resolution Terrestrial Lidar Scanning

In this work, the use of focused terrestrial lidar scanning enabled quantification of highly detailed spatial variability in the monthly evolution of two dune systems on an intermediate beach subject to a series of large storm events over a 2.5 year time period. The high-resolution 3D point clouds were used to quantify the simultaneous evolution of topographic and ecological characteristics on sub-meter scales. The detail of the resolved deposition characteristics in this study highlights the advantages of terrestrial lidar scanning relative to conventional topographic measurement approaches. For example, deposition in the northern site was shown to accumulate in concentrated zones: integrated volume changes at discrete cross-shore profiles within the 50 m alongshore stretch of coast studied varied by multiple m^3 over the multi-year timescales investigated (Figure 7a–d). This poses challenges for the use of conventional sparse cross-shore transect based analyses for representative morphologic characterization in complex coastal sites.

In addition to the high resolution which terrestrial lidar affords, this analysis highlighted the importance of frequent data collection. For example, the dune toe region at the north dune site varied at monthly scales; eroding or prograding depending on the hydrodynamic and meteorological details of individual storms (Figure 8). Without monthly surveys the deposition growth events would have been missed entirely since the north dune was net erosional over the course of the study. Similarly, without frequent observations which simultaneously quantified vegetation and bare earth elevation changes, the detailed relationships between deposition patterns and vegetation coverage could not have been quantified. Thus, observations at these high spatial and temporal resolutions are necessary to fully characterize the relevant eco-morphodynamic processes driving coastal change.

Additionally, in contrast to some dissipative coastal beaches which may accrete upwards of $10 \, m^3/m/yr$ [26,49] the net dune growth rates are much lower on this intermediate beach. In the 2015 to 2017 study period at the FRF, there were few storm events which grew the dune more than $1 \, m^3/m$ (Figure 7). This coincided with local deposition of sediment that was often only a few centimeters to a decimeter (Figures 5c,d, 8 and 11a,b), except in the sand deposit zones on the north dune crest where sediment deposition was often larger. These scales of change are relatively small and are within the uncertainty of airborne lidar or walking RTK transects (particularly on steep dune faces). While the recent increase in use of unmanned aircraft systems (UAS) coupled with structure-from-motion algorithms for measuring coastal beach topography (e.g., [78,91]) represents a marked step forward in our ability to characterize detailed three-dimensional coastal dune evolution [92], there remain challenges in obtaining high-accuracy, consistent data in many coastal settings. For example, it is sometimes unclear what elevation is returned on densely vegetated dune faces and differences between UAS and lidar point clouds can range from 0.5 to 1 m (see [93] for an example at the south dune site). Except in the presence of very dense vegetation, lidar-based systems can obtain bed points through the vegetation canopy, and therefore do not suffer from the same challenges as UAS technologies. Thus, this work demonstrates that high-frequency terrestrial lidar scanning approaches, which can be collected in either stationary [52,53,55,56,65] or mobile [54,87] setups, provide data at resolutions suitable for advancing our understanding of coastal morphodynamics and for improving coastal management approaches.

6. Conclusions

In this study, two 50 m segments of dune on an intermediate beach were monitored monthly with a terrestrial lidar scanner. Topographic changes and vegetation coverage were quantified at high spatial resolution (0.1 m in the alongshore and cross-shore dimensions) and used to investigate dune response to a series of major tropical and extratropical storm events. Both dune systems experienced similar aeolian and hydrodynamic forcing and had similar sediment types, but responded oppositely

(net accretional vs. net erosional) during the two years of observations, suggesting the details of each systems geomorphic and ecological properties at scales of 0.1 to 100 s of meters modulated their response. In general, storm events (high-wind and high waves) grew the south dune, but eroded the north dune. During most storms, waves collided with the north dune, leading to erosion of the dune face and removal of vegetation. However, in some storms, when wind was strong and obliquely onshore, the north dune did grow. Growth was confined largely at or within 3 m leeward of the vegetated dune crest at the two edges of the study site or near the dune toe. Some growth did occur on the steep dune face, but only when and where vegetation was consistently present. In contrast, the south dune grew consistently during the study, particularly during large wind events. Growth was concentrated on the vegetated dune face, which was more mildly sloped than the north dune. Deposition frequency decreased with increasing elevation on the dune face and increasing spatial vegetation coverage, whereas deposition magnitude reached a local maximum on the mid to upper dune face. This work demonstrated the added value of high-resolution terrestrial lidar scanning for quantifying detailed eco-morphodynamic feedbacks at highly resolved time and space scales.

References

1. Van Slobbe, E.; de Vriend, H.J.; Aarninkhof, S.; Lulofs, K.; de Vries, M.; Dircke, P. Building with Nature: In search of resilient storm surge protection strategies. *Nat. Hazards* **2013**, *66*, 1461–1480. [CrossRef]

2. Hanley, M.; Hoggart, S.; Simmonds, D.; Bichot, A.; Colangelo, M.; Bozzeda, F.; Heurtefeux, H.; Ondiviela, B.; Ostrowski, R.; Recio, M.; et al. Shifting sands? Coastal protection by sand banks, beaches and dunes. *Coast. Eng.* **2014**, *87*, 136–146. [CrossRef]

3. Bridges, T.S.; Burks-Copes, K.A.; Bates, M.E.; Collier, Z.A.; Fischenich, J.C.; Piercy, C.D.; Russo, E.J.; Shafer, D.J.; Suedel, B.C.; Gailani, J.Z.; et al. *Use of Natural and Nature-Based Features (NNBF) for Coastal Resilience*; US Army Engineer and Research Development Center: Vicksburg, MS, USA, 2015; ERDC SR015-1, p. 477.

4. Sutton-Grier, A.E.; Wowk, K.; Bamford, H. Future of our coasts: The potential for natural and hybrid infrastructure to enhance the resilience of our coastal communities, economies and ecosystems. *Environ. Sci. Policy* **2015**, *51*, 137–148. [CrossRef]

5. De Lillis, M.; Costanzo, L.; Bianco, P.; Tinelli, A. Sustainability of sand dune restoration along the coast of the Tyrrhenian Sea. *J. Coast. Conserv.* **2004**, *10*, 93–100. [CrossRef]

6. Grafals-Soto, R.; Nordstrom, K. Sand fences in the coastal zone: Intended and unintended effects. *Environ. Manag.* **2009**, *44*, 420–429. [CrossRef]

7. Nordstrom, K.F.; Jackson, N.L. Foredune restoration in urban settings. In *Restoration of Coastal Dunes*; Springer: Berlin/Heidelberg, Germany, 2013; pp. 17–31.

8. Harley, M.D.; Ciavola, P. Managing local coastal inundation risk using real-time forecasts and artificial dune placements. *Coast. Eng.* **2013**, *77*, 77–90. [CrossRef]

9. Biel, R.G.; Hacker, S.D.; Ruggiero, P.; Cohn, N.; Seabloom, E.W. Coastal protection and conservation on sandy beaches and dunes: Context-dependent tradeoffs in ecosystem service supply. *Ecosphere* **2017**, *8*. [CrossRef]

10. Kobayashi, N. Analytical solution for dune erosion by storms. *J. Waterw. Port Coast. Ocean Eng.* **1987**, *113*, 401–418. [CrossRef]

11. Morton, R.A.; Sallenger, A.H., Jr. Morphological impacts of extreme storms on sandy beaches and barriers. *J. Coast. Res.* **2003**, *19*, 560–573.

12. Larson, M.; Erikson, L.; Hanson, H. An analytical model to predict dune erosion due to wave impact. *Coast. Eng.* **2004**, *51*, 675–696. [CrossRef]

13. Priestas, A.M.; Fagherazzi, S. Morphological barrier island changes and recovery of dunes after Hurricane Dennis, St. George Island, Florida. *Geomorphology* **2010**, *114*, 614–626. [CrossRef]

14. Sallenger, A. Storm impact scale for barrier islands. *J. Coast. Res.* **2000**, *16*, 890–895.

15. Johnson, B.; Kobayashi, N.; Gravens, M. *Cross-Shore Numerical Model CSHORE for Waves, Currents, Sediment Transport and Beach Profile Evolution*; Technical Report Report ERDC/CHL-TR-12-22; U.S. Army Corps of Engineers Coastal Engineering Research Center: Vicksburg, MS, USA, 2012.

16. van Thiel de Vries, J.; Van Gent, M.; Walstra, D.; Reniers, A. Analysis of dune erosion processes in large-scale flume experiments. *Coast. Eng.* **2008**, *55*, 1028–1040. [CrossRef]

17. Cohn, N.; Ruggiero, P.; García-Medina, G.; Anderson, D.; Serafin, K.; Biel, R. Environmental and morphologic control on wave induced dune response. *Geomorphology* **2019**, *329*, 108–128. [CrossRef]

18. Splinter, K.D.; Kearney, E.T.; Turner, I.L. Drivers of alongshore variable dune erosion during a storm event: Observations and modelling. *Coast. Eng.* **2018**, *131*, 31–41. [CrossRef]

19. Overbeck, J.R.; Long, J.W.; Stockdon, H.F. Testing model parameters for wave-induced dune erosion using observations from Hurricane Sandy. *Geophys. Res. Lett.* **2017**, *44*, 937–945. [CrossRef]

20. Walker, I.J.; Davidson-Arnott, R.G.; Bauer, B.O.; Hesp, P.A.; Delgado-Fernandez, I.; Ollerhead, J.; Smyth, T.A. Scale-dependent perspectives on the geomorphology and evolution of beach-dune systems. *Earth-Sci. Rev.* **2017**, *171*, 220–253. [CrossRef]

21. Jackson, N.; Sherman, D.; Hesp, P.; Klein, A.; Ballasteros, F., Jr.; Nordstrom, K. Small-scale spatial variations in aeolian sediment transport on a fine-sand beach. *J. Coast. Res.* **2006**, *1*, 379–383.

22. Davidson-Arnott, R.G.; Yang, Y.; Ollerhead, J.; Hesp, P.A.; Walker, I.J. The effects of surface moisture on aeolian sediment transport threshold and mass flux on a beach. *Earth Surf. Process. Landforms* **2008**, *33*, 55–74. [CrossRef]

23. Sherman, D.J.; Li, B.; Farrell, E.J.; Ellis, J.T.; Cox, W.D.; Maia, L.P.; Sousa, P.H. Measuring aeolian saltation: A comparison of sensors. *J. Coast. Res.* **2011**, 280–290. [CrossRef]

24. de Vries, S.; Arens, S.; de Schipper, M.; Ranasinghe, R. Aeolian sediment transport on a beach with a varying sediment supply. *Aeolian Res.* **2014**, *15*, 235–244. [CrossRef]

25. Psuty, N. The coastal foredune: A morphological basis for regional coastal dune development. In *Coastal Dunes*; Martínez, M., Psuty, N., Eds.; Springer: Berlin, Germany, 2004; pp. 11–27.

26. de Vries, S.; Southgate, H.; Kanning, W.; Ranasinghe, R. Dune behavior and aeolian transport on decadal timescales. *Coast. Eng.* **2012**, *67*, 41–53. [CrossRef]

27. Ollerhead, J.; Davidson-Arnott, R.; Walker, I.J.; Mathew, S. Annual to decadal morphodynamics of the foredune system at Greenwich Dunes, Prince Edward Island, Canada. *Earth Surf. Process. Landforms* **2012**, *38*, 284–298. [CrossRef]

28. Cohn, N.; Ruggiero, P.; de Vries, S.; Kaminsky, G. New insights on the relative contributions of marine and aeolian processes to coastal foredune growth. *Geophys. Res. Lett.* **2018**, *45*, 4965–4973. [CrossRef]

29. Hoonhout, B.M.; de Vries, S. A process-based model for aeolian sediment transport and spatiotemporal varying sediment availability. *J. Geophys. Res. Earth Surf.* **2016**, *121*, 1555–1575. [CrossRef]

30. Bauer, B.O.; Davidson-Arnott, R.G. A general framework for modeling sediment supply to coastal dunes including wind angle, beach geometry, and fetch effects. *Geomorphology* **2003**, *49*, 89–108. [CrossRef]

31. Bauer, B.; Davidson-Arnott, R.; Hesp, P.; Namikas, S.; Ollerhead, J.; Walker, I. Aeolian sediment transport on a beach: Surface moisture, wind fetch, and mean transport. *Geomorphology* **2009**, *105*, 106–116. [CrossRef]

32. Delgado-Fernandez, I. A review of the application of the fetch effect to modelling sand supply to coastal foredunes. *Aeolian Res.* **2010**, *2*, 61–70. [CrossRef]

33. Short, A.; Hesp, P. Wave, beach and dune interactions in southeastern Australia. *Mar. Geol.* **1982**, *48*, 259–284. [CrossRef]

34. Buckley, R. The effect of sparse vegetation on the transport of dune sand by wind. *Nature* **1987**, *325*. [CrossRef]

35. Hesp, P. A review of biological and geomorphological processes involved in the initiation and development of incipient foredunes. *Proc. R. Soc. Edinburg B* **1989**, *96*, 181–201. [CrossRef]

36. Davidson-Arnott, R.G.; MacQuarrie, K.; Aagaard, T. The effect of wind gusts, moisture content and fetch length on sand transport on a beach. *Geomorphology* **2005**, *68*, 115–129. [CrossRef]

37. Moulton, M.A.; Hesp, P.A.; Miot da Silva, G.; Bouchez, C.; Lavy, M.; Fernandez, G.B. Changes in vegetation cover on the Younghusband Peninsula transgressive dunefields (Australia) 1949–2017. *Earth Surf. Process. Landforms* **2018**, *44*, 459–470. [CrossRef]

38. Cohn, N.; Hoonhout, B.M.; Goldstein, E.B.; De Vries, S.; Moore, L.J.; Durán Vinent, O.; Ruggiero, P. Exploring Marine and Aeolian Controls on Coastal Foredune Growth Using a Coupled Numerical Model. *J. Mar. Sci. Eng.* **2019**, *7*, 13. [CrossRef]

39. Roelvink, D.; Costas, S. Coupling nearshore and aeolian processes: XBeach and Duna process-based models. *Environ. Modell. Softw.* **2019**, *115*, 98–112. [CrossRef]

40. Zarnetske, P.L.; Hacker, S.D.; Seabloom, E.W.; Ruggiero, P.; Killian, J.R.; Maddux, T.B.; Cox, D. Biophysical feedback mediates effects of invasive grasses on coastal dune shape. *Ecology* **2012**, *93*, 1439–1450. [CrossRef]

41. Smyth, T.A.; Hesp, P.A. Aeolian dynamics of beach scraped ridge and dyke structures. *Coast. Eng.* **2015**, *99*, 38–45. [CrossRef]

42. Hesp, P.A.; Smyth, T.A. Nebkha flow dynamics and shadow dune formation. *Geomorphology* **2017**, *282*, 27–38. [CrossRef]

43. Hesp, P.A. The Formation of Shadow Dunes. *SEPM J. Sediment. Res.* **1981**, *51*. [CrossRef]

44. Durán, O.; Moore, L.J. Vegetation controls on the maximum size of coastal dunes. *Proc. Natl. Acad. Sci. USA* **2013**, *110*, 17217–17222. [CrossRef]

45. Sherman, D.J.; Bauer, B.O. Dynamics of beach-dune systems. *Prog. Phys. Geogr.* **1993**, *17*, 413–447. [CrossRef]

46. Sherman, D.J. Problems of scale in the modeling and interpretation of coastal dunes. *Mar. Geol.* **1995**, *124*, 339–349. [CrossRef]

47. Elko, N.; Brodie, K.; Stockdon, H.; Nordstrom, K.; Houser, C.; McKenna, K.; Moore, L.; Rosati, J.; Ruggiero, R.; Thuman, R.; Walker, I. Dune management challenges on developed coasts. *Shore Beach* **2016**, *84*, 15–28.

48. Sigren, J.M.; Figlus, J.; Highfield, W.; Feagin, R.A.; Armitage, A.R. The Effects of Coastal Dune Volume and Vegetation on Storm-Induced Property Damage: Analysis from Hurricane Ike. *J. Coast. Res.* **2018**, *34*, 164–173. [CrossRef]

49. Ruggiero, P.; Kaminsky, G.M.; Gelfenbaum, G.; Cohn, N. Morphodynamics of prograding beaches: A synthesis of seasonal- to century-scale observations of the Columbia River littoral cell. *Mar. Geol.* **2016**, *376*, 51–68. [CrossRef]

50. Houser, C.; Wernette, P.; Rentschlar, E.; Jones, H.; Hammond, B.; Trimble, S. Post-storm beach and dune recovery: Implications for barrier island resilience. *Geomorphology* **2015**, *234*, 54–63. [CrossRef]

51. Eisemann, E.R.; Wallace, D.J.; Buijsman, M.C.; Pierce, T. Response of a vulnerable barrier island to multi-year storm impacts: LiDAR-data-inferred morphodynamic changes on Ship Island, Mississippi, USA. *Geomorphology* **2018**, *313*, 58–71. [CrossRef]

52. de Vries, S.; Verheijen, A.; Hoonhout, B.; Vos, S.; Cohn, N.; Ruggiero, P. Measured spatial variability of beach erosion due to aeolian processes. In Proceedings of the Coastal Dynamics Conference 2017, Helsingør, Denmark, 12–16 June 2017.

53. Smith, A.; Gares, P.A.; Wasklewicz, T.; Hesp, P.A.; Walker, I.J. Three years of morphologic changes at a bowl blowout, Cape Cod, USA. *Geomorphology* **2017**, *295*, 452–466. [CrossRef]

54. Donker, J.; van Maarseveen, M.; Ruessink, G. Spatio-Temporal Variations in Foredune Dynamics Determined with Mobile Laser Scanning. *J. Mar. Sci. Eng.* **2018**, *6*, 126. [CrossRef]

55. O'Dea, A.; Brodie, K.; Hartzell, P. Continuous Coastal Monitoring with an Automated Terrestrial Lidar Scanner. *J. Mar. Sci. Eng.* **2019**, *7*, 37. [CrossRef]

56. Phillips, M.; Blenkinsopp, C.; Splinter, K.; Harley, M.; Turner, I. Modes of berm and beachface recovery following storm reset: Observations using a continuously scanning lidar. *J. Geophys. Res. Earth Surf.* **2019**. [CrossRef]

57. Palmsten, M.; Brodie, K. Spatial Variability of Coastal Foredune Evolution, Part B: Timescales of Years to Decades. *J. Mar. Sci. Eng.* **2019**, in review.

58. Stauble, D.K. *Long-Term Profile and Sediment Morphodynamics: Field Research Facility Case History*; Technical Report; Coastal Engineering Research Center: Vicksburg, MS, USA, 1992.

59. Plant, N.G.; Holman, R.A. Intertidal beach profile estimation using video images. *Mar. Geol.* **1997**, *140*, 1–24. [CrossRef]

60. Lippmann, T.; Holman, R. The spatial and temporal variability of sand bar morphology. *J. Geophys. Res. Ocean.* **1990**, *95*, 11575–11590. [CrossRef]

61. Lee, G.H.; Nicholls, R.J.; Birkemeier, W.A. Storm-driven variability of the beach-nearshore profile at Duck, North Carolina, USA, 1981–1991. *Mar. Geol.* **1998**, *148*, 163–177. [CrossRef]

62. van Gaalen, J.F.; Tebbens, S.F.; Barton, C.C. Longshore sediment transport directions and rates from northern Maine to Tampa Bay, Florida: Literature compilation and interpretation. *J. Coast. Res.* **2016**, *32*, 1277–1301. [CrossRef]

63. Birkemeier, W.; Dolan, R.; Fisher, N. The evolution of a barrier island: 1930–1980. *Shore Beach* **1984**, *52*, 2–12.

64. Pianca, C.; Holman, R.; Siegle, E. Shoreline variability from days to decades: Results of long-term video imaging. *J. Geophys. Res. Ocean.* **2015**, *120*, 2159–2178. [CrossRef]

65. Conery, I.; Brodie, K.; Spore, N.; Walsh, J. Terrestrial lidar monitoring of coastal foredune evolution in managed and unmanaged systems. *Earth Surf. Process. Landforms* **2019**, in review.

66. LeWinter, A. Characterization of the Overlook Crater and Lava Lake of Kīlauea Volcano through Terrestrial Laser Scanning. Master's Thesis, University of Northern Colorado, Greeley, CO, USA, 2014.

67. Ruggiero, P.; Kaminsky, G.M.; Gelfenbaum, G.; Voigt, B. Seasonal to Interannual Morphodynamics along a High-Energy Dissipative Littoral Cell. *J. Coast. Res.* **2005**, *213*, 553–578. [CrossRef]

68. Gelfenbaum, G.; Stevens, A.W.; Miller, I.; Warrick, J.A.; Ogston, A.S.; Eidam, E. Large-scale dam removal on the Elwha River, Washington, USA: Coastal geomorphic change. *Geomorphology* **2015**, *246*, 649–668. [CrossRef]

69. Stockdon, H.F.; Doran, K.S.; Sallenger, A.H. Extraction of Lidar-Based Dune-Crest Elevations for Use in Examining the Vulnerability of Beaches to Inundation During Hurricanes. *J. Coast. Res.* **2009**, *10053*, 59–65. [CrossRef]

70. Yates, M.L.; Guza, R.T.; O'Reilly, W.C.; Hansen, J.E.; Barnard, P.L. Equilibrium shoreline response of a high wave energy beach. *J. Geophys. Res.* **2011**, *116*. [CrossRef]

71. Davidson, M.; Splinter, K.; Turner, I. A simple equilibrium model for predicting shoreline change. *Coast. Eng.* **2013**, *73*, 191–202. [CrossRef]

72. Davidson-Arnott, R.; Hesp, P.; Ollerhead, J.; Walker, I.; Bauer, B.; Delgado-Fernandez, I.; Smyth, T. Sediment Budget Controls on Foredune Height: Comparing Simulation Model Results with Field Data. *Earth Surf. Process. Landforms* **2018**. [CrossRef]

73. Holman, R.; Stanley, J. The history and technical capabilities of Argus. *Coast. Eng.* **2007**, *54*, 477–491. [CrossRef]

74. Levy, G.F. *Vegetative Study at the Duck Field Research Facility, Duck, North Carolina*; Technical Report; Old Dominion University, Department of Biological Sciences: Norfolk, VA, USA, 1976.

75. Goldstein, E.B.; Mullins, E.V.; Moore, L.J.; Biel, R.G.; Brown, J.K.; Hacker, S.D.; Jay, K.R.; Mostow, R.S.; Ruggiero, P.; Zinnert, J. Literature-based latitudinal distribution and possible range shifts of two US east coast dune grass species (Uniola paniculata and Ammophila breviligulata). *PeerJ* **2018**, *6*, e4932. [CrossRef]

76. Arens, S.M. Patterns of sand transport on vegetated foredunes. *Geomorphology* **1996**, *4*, 339–350. [CrossRef]

77. Hesp, P.A.; Walker, I.J.; Chapman, C.; Davidson-Arnott, R.; Bauer, B.O. Aeolian dynamics over a coastal foredune, Prince Edward Island, Canada. *Earth Surf. Process. Landforms* **2013**, *38*, 1566–1575. [CrossRef]

78. Laporte-Fauret, Q.; Marieu, V.; Castelle, B.; Michalet, R.; Bujan, S.; Rosebery, D. Low-Cost UAV for High-Resolution and Large-Scale Coastal Dune Change Monitoring Using Photogrammetry. *J. Mar. Sci. Eng.* **2019**, *7*, 63. [CrossRef]

79. Delgado-Fernandez, I.; Davidson-Arnott, R. Meso-scale aeolian sediment input to coastal dunes: The nature of aeolian transport events. *Geomorphology* **2011**, 217–232. [CrossRef]

80. Lynch, K.; Jackson, D.W.; Cooper, J.A.G. Foredune accretion under offshore winds. *Geomorphology* **2009**, *105*, 139–146. [CrossRef]

81. Bauer, B.O.; Davidson-Arnott, R.G.D.; Walker, I.J.; Hesp, P.A.; Ollerhead, J. Wind direction and complex sediment transport response across a beach-dune system. *Earth Surf. Process. Landforms* **2012**, *37*, 1661–1677. [CrossRef]

82. Walker, I.J.; Hesp, P.A.; Davidson-Arnott, R.G.D.; Ollerhead, J. Topographic Steering of Alongshore Airflow over a Vegetated Foredune: Greenwich Dunes, Prince Edward Island, Canada. *J. Coast. Res.* **2006**, *22*, 1278–1291. [CrossRef]

83. Walker, I.J.; Hesp, P.A.; Davidson-Arnott, R.; O.Bauer, B.; Namikas, S.L.; Ollerhead, J. Responses of three-dimensional flow to variations in the angle of incident wind and profile form of dunes: Greenwich Dunes, Prince Edward Island, Canada. *Geomorphology* **2009**, *105*, 127–138. [CrossRef]

84. Hesp, P.A.; Smyth, T.A.; Nielsen, P.; J.Walker, I.; O.Bauer, B.; Davidson-Arnott, R. Flow deflection over a foredune. *Geomorphology* **2015**, *230*, 64–74. [CrossRef]

85. Guedes, R.; Bryan, K.R.; Coco, G.; Holman, R.A. The effects of tides on swash statistics on an intermediate beach. *J. Geophys. Res.* **2011**, *116*. [CrossRef]

86. Soldini, L.; Antuono, M.; Brocchini, M. Numerical Modeling of the Influence of the Beach Profile on Wave Run-Up. *J. Waterw. Port Coast. Ocean Eng.* **2013**, *139*, 61–71. [CrossRef]

87. Brodie, K.L.; Spore, N.J. Foredune classification and storm response: Automated analysis of terrestrial lidar DEMs. In Proceedings of the Coastal Sediments 2015, San Diego, CA, USA, 11–15 May 2015; World Scientific: Singapore, 2015.

88. Wiedemann, A.M.; Pickart, A. TheAmmophila problem on the Northwest coast of North America. *Landsc. Urban Plan.* **1996**, *34*, 287–299. [CrossRef]

89. Mullins, E.; Moore, L.J.; Goldstein, E.B.; Jass, T.; Bruno, J.; Durán Vinent, O. Investigating dune-building feedback at the plant level: Insights from a multispecies field experiment. *Earth Surf. Process. Landforms* **2019**. [CrossRef]

90. Jackson, N.L.; Nordstrom, K.F. Aeolian sediment transport and landforms in managed coastal systems: A review. *Aeolian Res.* **2011**, *3*, 181–196. [CrossRef]

91. Mancini, F.; Dubbini, M.; Gattelli, M.; Stecchi, F.; Fabbri, S.; Gabbianelli, G. Using unmanned aerial vehicles (UAV) for high-resolution reconstruction of topography: The structure from motion approach on coastal environments. *Remote Sens.* **2013**, *5*, 6880–6898. [CrossRef]

92. Ruessink, B.; Arens, S.; Kuipers, M.; Donker, J. Coastal dune dynamics in response to excavated foredune notches. *Aeolian Res.* **2018**, *31*, 3–17. [CrossRef]

93. Brodie, K.L.; Bruder, B.L.; Slocum, R.K.; Spore, N.J. Simultaneous Mapping of Coastal Topography and Bathymetry from a Lightweight Multi-Camera UAS. *IEEE Trans. Geosci. Remote Sens.* **2019**, in press.